

JOHNSON GRANT  
IN-34-CR

124545  
54P.

COMPUTATIONAL FLUID DYNAMICS  
AND AEROTHERMODYNAMICS

# aerospace engineering department



Semianual Progress Report  
July 1987 - December 1987

## TEXAS A&M UNIVERSITY

TAMRF Report No. 5671-88-01

March 1988

NASA Grant No. NAG 9-192  
TAMRF Project RF 5671

Leland A. Carlson  
Professor of Aerospace Engineering  
Texas A&M University  
College Station, Texas 77843-3141

(NASA-CR-182490) COMPUTATIONAL FLUID  
DYNAMICS AND AEROTHERMODYNAMICS Semiannual  
Progress Report, Jul. - Dec. 1987 (Texas  
A&M Univ.) 54 P

N88-16989

CSCL 20D

Unclassified  
G3/34 0124545

TEXAS ENGINEERING EXPERIMENT STATION

**COMPUTATIONAL FLUID DYNAMICS  
AND AEROTHERMODYNAMICS**

**Semiannual Progress Report**

**July 1987 -- December 1987**

**TAMRF Report No. 5671-88-01**

**March 1988**

**NASA Grant No. NAG 9-192  
TAMRF Project RF 5671**

**Leland A. Carlson  
Professor of Aerospace Engineering  
Texas A&M University  
College Station, TX 77843-3141**

## COMPUTATIONAL FLUID DYNAMICS AND AEROTHERMODYNAMICS

(Development of Nonequilibrium Models Applicable to AOTV/AFE and Superorbital Flight Regimes)

### I. Introduction

This report covers the period from July 1, 1987 thru December 31, 1987. It will briefly describe the current status of the project and the research effort during the last six months. Since most of these activities have been summarized in two extended abstracts of papers to be presented at the AIAA Thermophysics Meeting in June 1988, these abstracts are included as appendices.

### II. Status and Personnel

Due to the delayed start on the project, the present effort has been officially extended until 2 June 1988. Currently, the project is essentially on schedule and most of the work should be completed prior to the end of May 1988. However, to allow proper preparation of final reports, attendance at the AIAA Thermophysics Meeting, etc. an additional extension until the end of August 1988 will be requested.

At the present time, the staff associated with the project are Leland A. Carlson, Principal Investigator, and Glenn Bobskill, Robert Greendyke, and Thomas Gally, Graduate Research Assistants. The research work associated with this project will form the basis of the Masters theses of Mr. Bobskill and Mr. Greendyke, both of whom should finish in May 1988. Mr. Gally is currently working on his doctoral degree and his present research efforts have been split between this project and one involving transonic wing design and analysis.

### III. Research Progress

As indicated in the last progress report, the project is organized into two efforts. The first involves the development of an approximate stagnation point solution, while the second is directed towards the study of nonequilibrium models for vibration-dissociation chemical reaction coupling and electron temperature and radiation approximations. Most of the efforts of the last six months in these two areas has been conveniently summarized in two extended abstracts submitted to the 1988 AIAA Thermophysics Meeting. Consequently, these two abstracts are included as appendices to this report. For your information, both papers have been accepted for presentation at the meeting.

In addition to the work reported in Appendix II concerning nonequilibrium model studies, a considerable amount of additional progress has occurred. For example, as shown on Table I, a second chemical reaction model has been developed which includes 10 species and 11 reactions instead of the seven species six reactions discussed in the appendix. This new model is still very simple and yet should permit some reasonable comparisons of the effects of including or excluding various species in the computation of AOTV/AFE flowfields.

In addition, as shown on Table II, the current inviscid nonequilibrium blunt body computer code has five different vibrational-chemistry coupling models and for use in radiative heat transfer calculations four absorption coefficient models. In addition, approximate nonequilibrium correction factors have been developed for these radiation models. Obviously, with these choices a wide variety of model combinations can be studied and the effects of using various models can be determined.

It should be noted that the nonequilibrium radiation correction factors are based upon assumptions concerning the nature of the excited electron states of the atoms and the molecules and attempt to include the effects of the possible nonexistence of local thermodynamic equilibrium between the electronic states during the nonequilibrium chemistry relaxation process.

Some preliminary radiative heat transfer results for a point on the AFE approximately nine centimeters above the stagnation point are shown on Table III. The flight conditions for this case were 10 Km/sec at 80 Km.; and the results shown on the table do not include any nonequilibrium radiation correction factors. Thus, they essentially assume that LTE exists between excited states; and the results should be viewed as the maximum possible radiative heat transfer (within the limitations of each model). It should be noted that the 5-Step and 2-Step models are essentially based upon atomic nitrogen only while the radiance and 8-Step models include atomic nitrogen and oxygen and also molecular contributions. While these results indicate significant contributions from the VUV, it might be possible that the cool layer near the wall (not included in the present inviscid model) will absorb a considerable portion of the UV and VUV radiation.

In addition, it should be noted that preliminary results including the nonequilibrium radiation correction factors predict significantly lower values on the order of one to 10 watts/sq. cm. While these results are very preliminary, it does appear that nonequilibrium effects on the radiative transfer are extremely important for this flight condition.

Further, some very interesting preliminary results have been obtained using two different reaction rates for the electron nitrogen impact ionization reaction. The first rate is based upon experimental results of Wilson (Ref. 1); while the second, which is two orders of magnitude faster, is the one recommended by Kang and Dung. When applied to the AFE shape at 10 Km/sec and at 80 Kilometers, the use of the second rate constant significantly increases the amount of ionized nitrogen and decreases the amount of atomic nitrogen in the shock layer. Also, the results with the second rate indicate significantly more molecular nitrogen than those obtained using the first rate. Apparently, during the middle and late stages of relaxation, the dissociation of nitrogen is strongly affected by the decrease in atomic nitrogen. (During early stages nitrogen dissociation is primarily affected by shuffle reactions involving O and NO.) The effect of these differences on radiative heat transfer is currently being investigated and will be reported upon at a later date.

#### IV. Future Efforts

During the next reporting period, work will continue on investigating the usage of various models in computing AFE/AOTV flowfields. Particular attention will be devoted to obtaining results for AFE trajectory points typical of entry and the max-Q point.

#### V. References

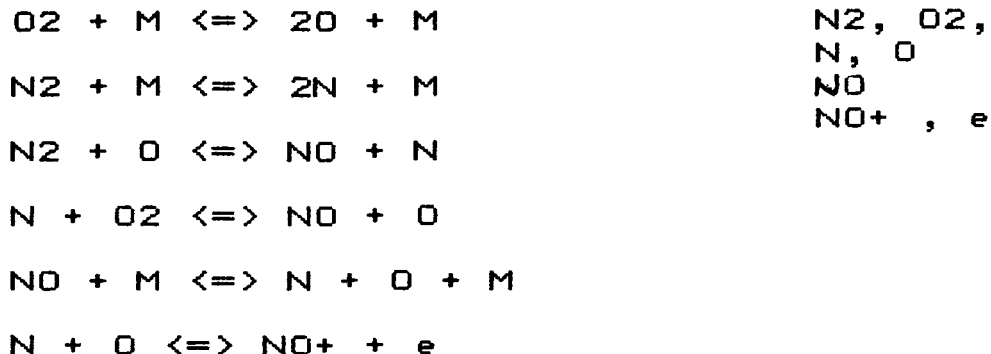
1. Wilson, J. "Ionization Rate of Air behind High-Speed Shock Waves," Physics of Fluids, Vol. 9, No. 10, October 1966, pp. 1913-1921.

#### III. Grant Monitor

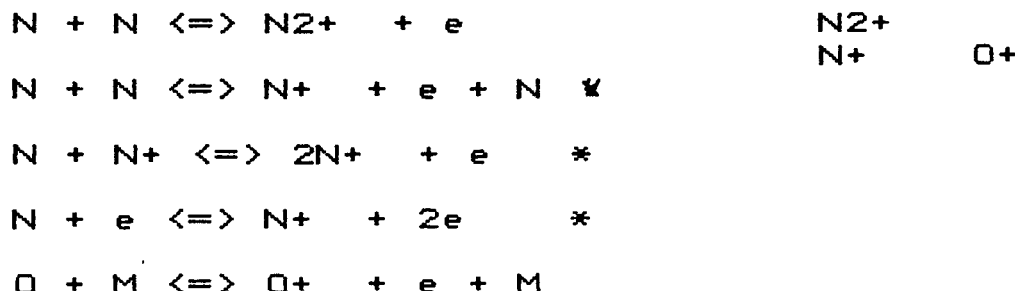
The NASA Technical Monitor for this project is Dr. Carl Scott, Mail Code ED8, NASA Johnson Space Center, Houston, Texas, 77058.

## Current Reaction Models

### A. 7 Species 6 reactions



### B. Extend to 10 species, 11 reactions



\* -- These should involve excited state effects.

Goal: Keep as simple as possible.

TABLE I

## Vibration-Chemistry Coupling Models

1. Vibrational Equilibrium
2. CVD
3. CVDV
4. CVDV Preferential
5. Park-Like Model

## Radiation Models

1. Radiance (Cornell)
2. Two-Step Air (Anderson)
3. Five-Step Nitrogen (Knott, Carlson, and Nerem)
4. Eight-Step Air (Olstad)

Used in tangent slab approximation with local concentrations and Te and with and without nonequilibrium correction factors.

TABLE II

RADIATIVE HEAT TRANSFER  
Approx. 9 cm above Stagnation Point  
(No Corrections)

	CVDU (7S6R)	Park-Like (7S6R)	CVDU (10S11R)
<b>Radiance Model</b>			
N(2000-5000)	217	2	155
N(500-2000)	4046	697	3221
O(2000-5000)	170	3	124
O(500-2000)	1488	320	1199
plus 8 others			
Total	5921	1021	4700
<b>5 Step Model</b>			
620-1100	129	9	39
1100-1300	171	3	128
1300-1570	3107	121	2407
1570-7870	240	1	165
7870-9557	244	6	182
Total	3892	141	2922
<b>8 Step Model</b>			
400-852	49	0	15
852-911	451	8	349
911-1020	1556	18	1169
1020-1130	526	5	382
1130-1801	2809	43	2094
1801-4000	1578	75	1336
4000-	938	61	777
Total	7906	210	6121
<b>2 Step Model</b>			
0-1100	2805	55	2174
1100-	295	0	215
Total	3101	55	2388

TABLE III

## APPENDIX I

Approximations for Hypervelocity Nonequilibrium Radiating, Reacting, and Conducting Stagnation Regions

# APPROXIMATIONS FOR HYPERVELOCITY NONEQUILIBRIUM RADIATING, REACTING, AND CONDUCTING STAGNATION REGIONS

Leland A. Carlson\*  
Texas A&M University  
College Station, Texas 77843-3141  
(409)845-1426

(Submitted for Presentation at the AIAA Thermophysics, Plasmadynamics, and Lasers Conference, June 27-29, 1988, San Antonio, Texas)

## EXTENDED ABSTRACT

### Introduction

In the future aero-assisted orbital transfer vehicles (AOTVs) will be used to operate, supply, maintain, and man satellites and space stations and to return from lunar and Mars missions. Those vehicles descending from geosynchronous to high or low earth orbit will operate in the entry and aero-assisted mode at velocities ranging from 7 to 11 Km/sec at altitudes of 70 to 100 km., with a nominal entry velocity of 10 Km/sec and peak dynamic pressure occurring at 75 km. Likewise, AOTVs returning from the Moon or Mars will enter at higher nominal velocities, 11 km/sec for lunar return and 13.5 to 16 Km/sec for Martian return; and, thus, they will have a wider operating range from 7 to 18 Km/sec at 60 to 100 km.

Obviously, in order to efficiently design and operate such vehicles not only must the important factors affecting the vehicle flowfields be understood but also methods for rapidly predicting them must be available. While the corner and afterbody flows for such vehicles are complicated and highly rotational and viscous, the forebody flow structure thru much of the entry flight profile is dominated by nonequilibrium chemistry and radiation; and these phenomena will significantly affect the heat transfer to and perhaps the aerodynamics of the vehicle.

In many cases, detailed three dimensional nonequilibrium viscous computations of AOTV flowfields will be required in order to obtain complete understanding of various phenomena or to finalize a design. Such detailed computations, typically using the Navier-Stokes equations (Ref. 1), are extremely lengthy often requiring many hours of supercomputer time; and, thus, they are not suitable for quick studies, the determination of design trends, parametric studies, etc. In addition, while some of these methods include nonequilibrium chemistry, few include the effects of such nonequilibrium phenomena as vibration dissociation coupling and electron thermal nonequilibrium; and because

---

\* Professor of Aerospace Engineering, Associate Fellow AIAA.

of their lengthy computational times, these detailed methods are unwieldy for evaluating or developing models and approximations representing these nonequilibrium phenomena. Further, only a few have attempted to include radiative heat transfer; and these have either used very detailed nonequilibrium radiation models under conditions without significant radiation gasdynamic coupling (Ref. 2) or they have, perhaps inappropriately, utilized equilibrium radiation models under nonequilibrium conditions (Ref. 3-4), assuming that the usage of local concentrations and temperatures is sufficient to handle nonequilibrium radiation.

This paper will discuss one portion of an effort to evaluate and develop models and approximations for nonequilibrium chemical and radiating flows associated with AOTVs returning from orbital, lunar, and Martian missions and will be applicable to entry velocities ranging from 10.5 Km/sec to 18 Km/sec. (Reference 5 will present results associated with the 7 - 10 Km/sec regime.) The objectives of this paper are to investigate various approximations that can be used in analyzing radiating, reacting, and conducting shock layers, and to develop a rapid stagnation point solution technique that is suitable for parametric studies, and, perhaps, for evaluating and testing various nonequilibrium radiation models. It should be noted that the approximations discussed in this paper need not always be applied simultaneously. Also the resultant techniques are applied to the stagnation zone only as an initial effort. Many of them can, in principle, be extended to multi-dimensional and entry vehicle flowfields.

#### Approximate Solution

The primary equations governing the radiating reacting flow behind a hypervelocity shock wave are the global energy equation,

$$\rho u \frac{dh}{dx} + \frac{d}{dx} \left[ \sum_{i=1}^s (-\lambda_i \frac{dT_i}{dx}) \right] + \frac{d}{dx} \left[ \sum_{i=1}^s \rho_i U_i h_i \right] + \frac{d q_E}{dx} - u \frac{dp}{dx} = - \sum_{i=1}^s w_i h_i^0 \quad (1)$$

and the equation of radiative transfer. Normally these equations must be solved in conjunction with the conservation equations for species mass, momentum, and electron energy, etc. and because the radiative transfer depends upon the flowfield solution, either the problem must be solved as a "time dependent" type of problem or iteration on the entire flowfield must be performed. With the introduction of chemical nonequilibrium, many flowfield points should be calculated in the immediate postshock region and near the wall in order to represent the large temperature and species concentration gradients which exist in those regions; and this requirement coupled with the complication of including radiative transfer usually results in long computational times.

Based upon previous detailed solutions (Ref. 2,4, 6-9), several distinctive features for radiating reacting hypervelocity stagnation region shock layers in the 11-18 Km/sec range can be determined; and these are schematically represented on the sketch below.

II Conducting	I Conducting	IV
II Chemically Relaxing	I Chemical Equilibrium	IV
II (Ionization)	I	IV
II u very small	u very small	IV
II p approx. constant	I p approx. constant	IV
II Te approx. constant	I Radiative Losses From Optically Thin Part of the Spectrum	IV
II Radiative Transfer	I	IV
II Dominated by	I	IV
II Spectral Regions	I	IV
II Having Large	I	IV
II Absorption Coefficients	Te = TH	IV
II	I	IV
II Te $\neq$ TH	I	IV
Bow Shock Wave	End of Nonequilibrium Zone	Wall

Typically the shock layer is composed of a chemical relaxation zone immediately behind the shock front that is dominated by first ionization since at the velocities being considered dissociation is complete in the shock front (Ref. 4 and 10). While in this region the electron temperature is not equal to the heavy particle temperature, it is relatively constant. Also, most of the radiative losses occur from the ultra-violet, which is characterized by large absorption coefficients; and the large temperature gradients should make thermal conduction important. Downstream the flow should be in chemical and thermal equilibrium, and radiative energy losses should be associated with optically thin/transparent portion of the spectrum characterized by small absorption coefficients.

Due to the origin of the radiative losses, the radiative transfer can be represented by a thick-thin approximation similar to that formalized by OIstad (Ref. 11). This approach includes, at a point, only that part of the spectrum contributing significantly to radiative cooling. Thus, for the nonequilibrium relaxation region, the solution depends upon the radiative transfer from only those regions having large absorption coefficients. This zone will subsequently be referred to as the thick region and it will be characterized by the corresponding optical thickness coordinate,  $\tau_T$ . Likewise, the downstream equilibrium region will only include "transparent" radiation losses, will be called the thin region, and will be characterized by the optical thickness  $\tau_e$ . With this approach, solutions for each region can be obtained separately. This approach has been used in the past for equilibrium (Ref. 11) shock layers, and for frozen and reacting flow

behind normal shock waves (Ref. 12-13); and a related layering approach has been used for non-conducting nonequilibrium flows (Ref. 8).

(For the purposes of the abstract, many details will be omitted in the following discussion. The final paper will contain a complete discussion and, where appropriate, the necessary justifications.) Based upon the above discussion and sketch, several simplifying approximations can be made. Specifically, assuming dissociation complete in the shock front, ambipolar diffusion, constant post shock pressure, and that in the nonequilibrium zone that the electron temperature is constant, the energy equation can be uncoupled from the momentum equation and the electron energy equation. Next, the equation can be "uncoupled" from the continuity equation by using the transformation of Goulard (Ref. 14)

$$d\bar{n} = \bar{\rho}^{1/2} d\bar{x} \quad \bar{\rho} \bar{u} = -\bar{n} \quad (2)$$

which has been shown to be approximately true even in the viscous radiating case (Ref. 15).

Then, if the equation is transformed to an optical depth coordinate system via

$$d\gamma_i = \frac{K_i L}{\bar{\rho}^{1/2}} \quad (3)$$

under the assumptions of constant Prandtl number and that  $\bar{\rho}^{1/2} \bar{\mu} = 1$  it is even further simplified. However, it still contains thermal conduction, radiative transfer, chemical and thermal nonequilibrium, and a variable absorption coefficient. In the spirit of the thick-thin approximation, the latter in the thick chemically reacting zone immediately behind the shock front can be approximated as

$$K_T = K_{T_s} \bar{\rho}^{1/2} \quad (4)$$

where  $K_{T_s}$  is the absorption coefficient of the thick nonequilibrium zone evaluated immediately behind the shock front using the electron temperature and assuming dissociation complete in the front. This approximation corresponds to assuming a constant absorption cross section for the region, and yet it retains via the density dependence the dependence of  $K_T$  upon the flow properties.

Next, since it is assumed that the radiative transfer in the thick zone is dominated by spectral regions having large absorption coefficients, these regions can be represented as a gray gas step

$$-\frac{d\dot{g}_{Ri}}{dx} = -4\pi K_i S_i + 2\pi K_i \int_0^w S_i E_i(\gamma_i \cdot z_i) dz \quad (5)$$

This expression can be approximated in the thick region by replacing  $E_i(x)$  with the exponential approximation  $2\exp(-2x)$  and by representing the regional source function,  $S_T$ , as a constant,  $S_{T_s}$ , at the post

shock value since the electron temperature is assumed constant in the thick region. Thus, for the thick region

$$-\frac{dg_{RT}}{dx} = -2\pi K_T S_{T_s} e^{-2\zeta_T} \quad (6)$$

The energy equation for the nonequilibrium zone can be further approximated and "uncoupled" from the chemistry by assuming that the degree of ionization,  $\epsilon$ , can be represented as

$$\rho_I/\rho = \epsilon = \epsilon_{eq} (1 - e^{-B\zeta_T}) \quad (7)$$

where  $\epsilon_{eq}$  is the downstream equilibrium condition and B is determined by correlation with experimental relaxation data (Ref. 10). This form is based upon previous detailed results (Ref. 4, 6-9) and should yield phenomenologically correct profiles. The important point is that it uncouples the species production and energy equations and permits a solution of the latter.

Thus, for the nonequilibrium thick region immediately behind the shock front the approximate energy equation is

$$\frac{A}{RePr} \bar{h}'' - (1 - \frac{\zeta_T}{A}) \bar{h}' = \Gamma_T e^{-2\zeta_T} + \left[ (1 - \frac{\zeta_T}{A}) C - \frac{A}{RePr} D \right] e^{-B\zeta_T} \quad (8)$$

$$\text{where } A = k_{T_s} L \quad \Gamma_T = \frac{2\pi S_T}{\rho_s u_{shs}} \quad C = (\bar{h}_I^\infty - \bar{h}_n^\infty) \epsilon_{eq} \cdot B$$

$$D = \bar{h}_e \epsilon_{eq} B^2 \quad Re = \frac{\rho_s u_{shs}}{L} \quad \bar{n} = 1 - \frac{\zeta_T}{A}$$

and all flow quantities have been nondimensionalized by appropriate post shock values immediately behind the front and the reference length L is the inviscid radiationless shock detachment distance if h is constant throughout the layer at the immediate completely dissociated but nonequilibrium post shock value. The appropriate boundary conditions for Eq. (8) are

$$\text{At } \zeta_T = 0 \quad \bar{h} = 1 + \frac{A}{RePr} \bar{h}' - \frac{A}{RePr} \bar{h}_e \epsilon_{eq} B \quad (9)$$

and

Downstream

$$\bar{h}_o = 1 - (\bar{h}_I^o - \bar{h}_A^o) \epsilon_{eq} - R_T \int_0^\tau \frac{e^{-\tau \gamma_T}}{1 - \frac{\gamma_T}{K_{T0} L}} d\gamma_T \quad (10)$$

Note that the shock boundary condition not only includes conduction effects (Ref. 16-17) but also indirectly includes radiative and chemical effects since it depends upon the form of the solution. Likewise, the downstream boundary condition corresponds to complete equilibrium accounting for energy losses due to radiation.

For the equilibrium or thin region between the wall and the end of the nonequilibrium zone, the absorption coefficient can be approximated as

$$k_t = k_{t0} \left( \frac{\bar{\rho}}{\rho_0} \right)^{1/2} \quad (11)$$

where the subscript 0 denotes conditions at the start of the thin region. Also in this region the radiative transfer can be approximated as

$$\frac{dq_R}{dx} = E_{t0} \left( \frac{\rho}{\rho_0} \right)^{1/2} \left( \frac{\bar{h}}{\bar{h}_0} \right)^3 \quad (12)$$

where  $E_{t0}$  is the radiative emission loss at the beginning of the thin zone.

Now for the equilibrium zone, it is approximately true for the conditions considered in this paper that the degree of ionization,  $\epsilon$ , can be represented as a function of nondimensional enthalpy in a series of linear segments. For this initial investigation since first ionization processes dominate the chemistry over most of the equilibrium zone, this relationship can be approximated as

$$\epsilon = a \bar{h} + b \quad (13)$$

and a and b can be selected to closely approximate air thermodynamic data. As a consequence the approximate differential equation for the thin equilibrium region is

$$\begin{aligned} \left[ 1 - \frac{\gamma_t}{\gamma_{twall}} \right] \left[ 1 + a(\bar{h}_I^o - \bar{h}_A^o) \right] \bar{h}' - \frac{\gamma_{twall} \bar{h}''}{R_e P_r} \\ = - \frac{R_t}{K_{T0} L} \left( \frac{\bar{h}}{\bar{h}_0} \right)^3 \end{aligned} \quad (14)$$

where the appropriate boundary conditions are upstream  $\bar{h}_0$  and at the wall,  $T=T_{wall}$ .

Eqs. (8) and (14) can be written in finite difference form to form sets of tridiagonal equations. The thin equation, Eq. (14), however, is nonlinear due to the radiation term and must be solved using a Newton-Raphson iterative technique. After solution, the physical coordinates corresponding to the optical depth scales used in the equations can be obtained from integration of the transformations.

Once the flowfield solution has been obtained, it can be used to compute radiative and convective heat transfer to the wall. For the radiation, it is convenient to represent the spectrum by a series of gray gas steps, i.e. <sup>shock</sup>

$$g_E(\gamma) = 2\pi \sum_i \int_0^{\infty} [sgn(\gamma_i - z_i)] S_i(z_i) E_i(1/\gamma_i - z_i) dz_i \quad (15)$$

In the present case, the five step spectral absorption cross section model of Reference 18 has been used and the  $E_i$  function has been approximated. However, since this gray gas step model was developed assuming the gas to be in chemical equilibrium, it must be modified before it can be applied to the nonequilibrium part of the stagnation layer. As will be shown in the complete paper, where  $K_i$  represent the absorption coefficient,  $N_A$  is the atom number density,  $\epsilon_i$  is the cross section,  $B_i$  is the Planck function for the step, and  $\epsilon$  is the degree of ionization, the corrections are as follows:

Region 1: 620-110 Å. Since most of the processes considered in this step are continuum involving the ground state,

$$K_1 = N_A \epsilon_1$$

$$S_1 = \frac{\epsilon^2}{1-\epsilon} \frac{1-\epsilon_{eg}}{\epsilon_{eg}^2} B_1$$

Region 2: 1100-1300. This region is not presently included but will be for the final paper.

Region 3: 1300-1570 Å. Since this region accounts for VUV lines and the lower state is not the ground state

$$K_3 = \frac{\epsilon^2}{1-\epsilon} \frac{1-\epsilon_{eg}}{\epsilon_{eg}^2} N_A \epsilon_3$$

$$S_3 = B_3$$

Region 4: 1570-7870 Å. This region includes continuum free-free and free-bound excited states. Thus

$$K_4 = \frac{\epsilon^2}{1-\epsilon} \frac{1-\epsilon_{eg}}{\epsilon_{eg}^2} N_A \epsilon_4$$

$$S_4 = B_4$$

Region 5: 7870- 9552 A. This region accounts for infrared line radiation. Thus

$$K_5 = \frac{\epsilon^2}{1-\epsilon} \frac{1-E_{eq}}{E_{eq}^2} N_A G$$

$$S_5 = B_5$$

In these expressions,  $E_{eq}$  represents the degree of ionization which would exist if the flow were in equilibrium at the local pressure and electron temperature. Notice that all of these corrections significantly reduce the source terms or the absorption coefficients in regions of nonequilibrium. Of course, any appropriate grey gas step model could be used. Other examples are given in References 19 and 20.

The above stagnation point formulation has been programmed in BASIC and solved for a variety of cases using an Apple II+ computer. Typical solution times using 100 points in the nonequilibrium thick region and 100 points in the thin equilibrium zone are:

Flowfield Solution and Plots: 40 seconds

Calculation of Radiative Heat

Transfer by 5 step model: 70 seconds

Write Output and Plot to Disk: 60 seconds.

In the final paper, details concerning the selection of input parameters etc. will be presented.

### Results (Preliminary)

In this section, a series of initial results will be presented and discussed. These results will be amplified considerably in the final paper.

The present approximate method has been applied to a series of cases for a freestream velocity of 16 Km/sec. These cases were selected to be approximately representative of a small to midsize Martian return AOTV or other hypervelocity entry vehicle having a nose radius around 200 cm. and a wall temperature of 1645 deg K; and results have been obtained for altitudes from 55 Km to 80 Km., in 5 Km increments. Figure 1 shows temperature and degree of ionization profiles for three different altitudes. On these figures, the solid curves are the thick (nonequilibrium) zone and the dotted portions are the thin (equilibrium) region. As can be seen on Figure 1(a), at the lower altitudes, the stagnation region is primarily in chemical equilibrium. However, the region is not isothermal and considerable radiative cooling is present

as indicated by the decrease in temperature and  $\epsilon$ . (The enthalpy is proportional to  $T(1+\epsilon)$ .) So the enthalpy decrease due to radiative cooling in this case is quite significant.) Note that the plotted temperature immediately behind the shock front is the temperature after dissociation and includes thermal conduction effects due to the boundary condition. For this particular solution, considerable sensitivity of the thick solution to step size was encountered and for the results shown 100 points were used in the thick zone. This type of sensitivity might be very important in Navier-Stokes codes which often use shock capturing and relatively coarse grids.

Figures 1(b) and (c) show similar results at 70 and 80 Km respectively. As would be expected, as altitude increases the post shock nonequilibrium zone and the wall thermal layer increase in size and the radiation cooling decreases. By 80 km. the entire stagnation layer is dominated by nonequilibrium and/or wall conduction effects.

One of the possible applications of the present approximate method is to determine the effects of various parameters on stagnation point radiative heat transfer. Figure 2 shows the variation of radiative heat transfer with altitude for the present series of cases. (Units on QR are watts/square centimeter.)

Now comparison of various step models (Ref. 18-20) indicate that they are in reasonable agreement when applied to conditions similar to those for which they were initially developed. Typically, these are pressures of 10-20 atmospheres and path lengths of 3 cm or less. Unfortunately, when they are applied to conditions such as the present 70 km case of subatmospheric pressure and a standoff distance of 11.4 cm, these step models give widely different answers, particularly for the vacuum ultra-violet continuum and VUV lines. This difference is in spite of the fact that all of them were developed using similar procedures and were designed to yield results (i.e. radiation cross sections) independent of pressure. Apparently the differences in f numbers, band widths, and number of bands in these models becomes significant at the high altitude hypervelocity conditions being considered. In this respect, the more recently obtained f numbers referred to in Ref. 21 could perhaps be used with the detailed radiation code of Ref. 22 to obtain better step models, particularly in the ultra-violet portion of the spectrum.

As a consequence of these possible discrepancies, the radiative heat transfer from the visible and infrared portions of the spectrum has been plotted separately on Figure 2. (The difference is essentially the UV contribution.) As can be seen, as the vehicle descends the predicted visible plus IR heat transfer changes by about four orders of magnitude while the percentage of the total radiative heat load due to the UV decreases.

In order to approximately obtain an indication of the effect of the wall thermal boundary layer on the radiative heat transfer, results

were obtained for the 70 km case assuming a wall temperature of 13000 deg. K. Comparison of this nearly isothermal result with the 1645 deg K wall temperature is important because several investigators have assumed that the "cool" wall thermal layer would absorb a significant amount of the radiation and shield the wall. The present results are as follows:

<u>Region</u>	<u><math>Q(1645)/Q(13000)</math></u>
VUV Continuum	0.001
VUV Lines	0.919
Visible	0.948
IR Lines	0.951

These data indicate that the VUV continuum radiation is indeed absorbed in the outer portion of the boundary layer and that, as expected, the visible and IR line contributions are essentially unaffected.

Conclusions about the VUV lines, however, are not obvious. Since the present approximate solution does not yet include molecules, it can only be stated that the present radiation model indicates that nitrogen atoms will not attenuate the VUV line radiation in the wall thermal boundary layer. The effect of molecular species on VUV line radiation needs to be determined since, as shown on Figure 2, the source of heat transfer could be very significant. With respect to the VUV, it should be noted that the measurements of Wood et al (Ref. 23) and recent computations for the Fire 2 vehicle by Bird (Ref. 24) and Sutton (Ref. 25) indicate significant stagnation point heating from the ultra-violet.

Since the magnitude of various radiative properties are uncertain, some parametric studies have been conducted at the nominal condition of 16 Km/sec at 70 km. As shown, a decrease in the radiation cross section for VUV lines reduced the total heating by 71%. On the other, hand doubling of the visible band radiative cross section only increased the heating in the visible and IR by 17.6 percent while an order of magnitude change caused a 110% change in the visible and IR contribution. However, since increased visible emission increases radiative cooling, the total heating for these cases was actually reduced by 3.6% and 22.2% respectively. Quite obviously, accurate radiative cross sections and models will have to be developed before total radiative heat transfer predictions can be accurately made for these conditions.

Finally, with respect to Figure 2, it should be noted that for the conditions shown predictions for convective heat transfer by the present approximate model are -- 55 Km, 587 watts/sq cm, log value 2.76; 70 Km, 226 watts/sq cm, log value 2.35, and 80 Km, 98 watts/sq cm (log value 1.99). These should be viewed at best as noncatalytic wall estimates. In any event, they indicate that for these conditions radiative heat transfer is probably the dominant mechanism.

Results showing the effect of shock detachment distance or vehicle nose radius on flowfield profiles and heat transfer are shown on Figures

3 and 4. (For the paper, Figure 3(a-c) will be combined on one plot.) As expected, as nose radius decreases a higher percentage of the shock layer is affected by nonequilibrium and thermal boundary layer phenomena which should be accompanied by a decrease in radiative heat transfer and an increase in convective heating. Figure 4(a) shows that the predicted total radiative heating decreases by over 60% as the detachment distance is decreased by a factor of 4. Notice that the rate of decrease is nonlinear due to primarily self absorption effects in the ultra-violet. The variation in the heating from the visible and IR parts of the spectrum is, however, almost linear indicating that these regions are for these conditions essentially optically thin. Finally, the predicted convective heating increased from 226 watts/sq cm for  $\delta_n = 11.42$  cm to 331 watts/sq cm at 5.75 cm to 477 watts/sq cm at  $\delta_n = 2.92$  cm, thus following the expected square root dependence on nose radius.

Unfortunately, very little experimental data exists for conditions applicable to the present model. However, data is available for the Fire 2 flight experiment. As a result the present model has been applied to the Fire 2 trajectory for the period from 1632 seconds after launch (11.36 Km/sec at 76.42 Km) until 1642 seconds (10.71 Km/sec at 55.48 Km); and the results are compared with the viscous shock layer computations of Gupta (Ref. 3), which agree very well with the flight data, for the radiative heat transfer in the visible and infrared regions. As can be seen, the agreement between the two sets of results is surprisingly good. It should also be noted that the present results are in reasonable agreement with the Fire2 DSMC computations of Bird (Ref. 24) not only in the visible and IR regime but also in the ultra-violet and for convective heat transfer.

In the final paper, additional parametric results covering a velocity range of 12 Km/sec to 18 Km/sec will be presented.

#### Summary

Approximations applicable to radiating, reacting, and conducting stagnation region of a hypervelocity vehicle have been incorporated into a method for rapidly obtaining approximate solutions. This solution utilizes a coordinate system based upon the origin of the radiative losses and includes in a phenomenologically correct manner the effects of chemical and thermal nonequilibrium, and nonequilibrium, nongray radiative transfer. Results have been presented which demonstrate the usefulness of the method and indicate which radiation parameters require further study and definition. Excellent comparisons have been obtained with published results for the Fire2 data.

#### Acknowledgement

The effort was primarily supported under a subportion of NASA Grant No. NAG 9-192 from the NASA Johnson Space Center. The grant monitor is Dr. Winston Goodrich, Aerosciences Branch.

### References

1. Gnoffo, P. and Greene, F. A., "A Computational Study of the Flowfield Surrounding the Aeroassist Flight Experiment Vehicle," AIAA Paper No. 87-1575, June 1987.
2. Park, C., "Assessment of Two-Temperature Kinetic Model for Ionizing Kinetic Model for Ionizing Air," Aiaa Paper No. 87-1574, June 1987.
3. Gupta, R. N., "Navier-Stokes and Viscous Shock-Layer Solutions for Radiating Hypersonic Flows," AIAA Paper No. 87-1576, June 1987.
4. Carlson, L. A., "Radiative Gasdynamic Coupling and Nonequilibrium Effects behind Reflected Shock Waves," AIAA Journal, Vol. 9, No. 5, May 1971, pp. 858-865.
5. Carlson ,L. A., Bobskill, G. and Greendyke, R., "Comparison of Vibration Dissociation Coupling and Radiative Heat Transfer Models for AOTV/AFE Flowfields," Submitted for presentation at the AIAA Thermophysics, Plasmadynamics, and Lasers Conference, June 1988.
6. Nelson, H.F. and Goulard, R., "Structure of Shock Waves with Nonequilibrium Radiation and Ionization," The Physics of Fluids, Vol. 12, No. 8, Aug. 1969, pp. 1605-1617.
7. Chapin, C.E., "Nonequilibrium Radiation and Ionization in Shock Waves," AA&ES 67-9, June 1967, Purdue Univ., Lafayette, Ind.
8. Foley, W. H. and Clarke, J. H., "Shock Waves Structured by Nonequilibrium Ionizing and Thermal Phenomena," The Physics of Fluids, Vol. 16, No.3, March 1973, pp. 373-383.
9. Carlson, L. A., "Radiative Cooling and Nonequilibrium Chemistry Coupling behind Normal Shock Waves," AIAA Journal, Vol. 10., No. 2, Feb. 1972, pp. 230232.
10. Wilson, J., "Ionization Rate of Air Behind High Speed Shock Waves," The Physics of Fluids, Vol. 9, No. 10, Oct. 1966, pp. 1913-1921.
11. Olstad, W. B., "A Thick Thin Approximation for Radiative Transfer," AIAA Paper 73-715, Palm Springs, Calif. 1973.
12. Carlson, L. A., "A Radiating-Conducting Thick-Transparent Normal Shock Solution," The Physics of Fluids, Vol. 15, No. 12, Dec. 1972, pp. 2150-2152.
13. Carlson, L. A., "Engineering Approximations for Radiating Nonequilibrium Shock Layers," AIAA Journal, Vol. 12, No. 6, June 1974, pp. 832-837.

14. Gouillard, R., "Preliminary Estimates of Radiative Transfer Effects on Detached Shock Layer," AIAA Journal Vol. 2, No. 3, March 1964, pp. 494-502.
15. Nerem, R. M., "An Approximate Analysis of Thermal Conduction and Radiative Transport in the Stagnation-Point Shock Layer," AIAA Journal, Vol. 4, No.3, March 1966, pp. 539-541.
16. Cheng, H. K., Fundamental Phenomena in Hypersonic Flow, edited by J. G. Hall, Cornell Univ. Press, Ithaca, N.Y., 1966, p. 90.
17. Schneider, W., "Effect of Radiation on Hypersonic Stagnation Flow at Low Density," Zeitschrift fur Fluogwissenschaften Vol. 18, Nos. 2-3, Feb. 1970, pp. 50-58.
18. Knott, P. R., Carlson, L. A., and Nerem, R. M., "A Further Note on Shock Tube Measurements of End Wall Radiative Heat Transfer in Air," AIAA Journal Vol. 7, NO. 11, Nov. 1969, pp. 2170-2172.
19. Olstad, W. B., "Nongray Radiating Flow about Smooth Symmetric Bodies," AIAA Journal, Vol. 9, No. 1, January 1971., pp. 122-130.
20. Page, W. A., Compton, D. L., Borucki, W. J., Ciffone, D. L. and Cooper, D. M., "Radiative Transport in Inviscid Nonadiabatic Stagnation Region Shock Layers," Progress in Astronautics and Aeronautics, Vol. 21, 19889, pp. 75-114.
21. Cooper, D. M., Private Communication via notes at "Nonequilibrium Gasdynamics" Short Course, AIAA, June 1987.
22. Park, C., "Calculation of Nonequilibrium Radiation in AOTV Flight Regimes," AIAA Paper No. 84-0306, 1984.
23. Wood, A. D., Hoshizaki, H., Andrews, J.C., and Wilson, K.H., "Measurements of the Total Radiant Intensity of Air," AIAA Journal, Vol. 7, No. 1, January 1969, pp. 130-139.
24. Bird, G. A., "Nonequilibrium Radiation During Re-Entry at 10 Km/sec", AIAA Paper no. 87-1543, June 1987.
25. Sutton, K., "Air Radiation Revisted," AIAA Paper No. 84-1733, June 1984.

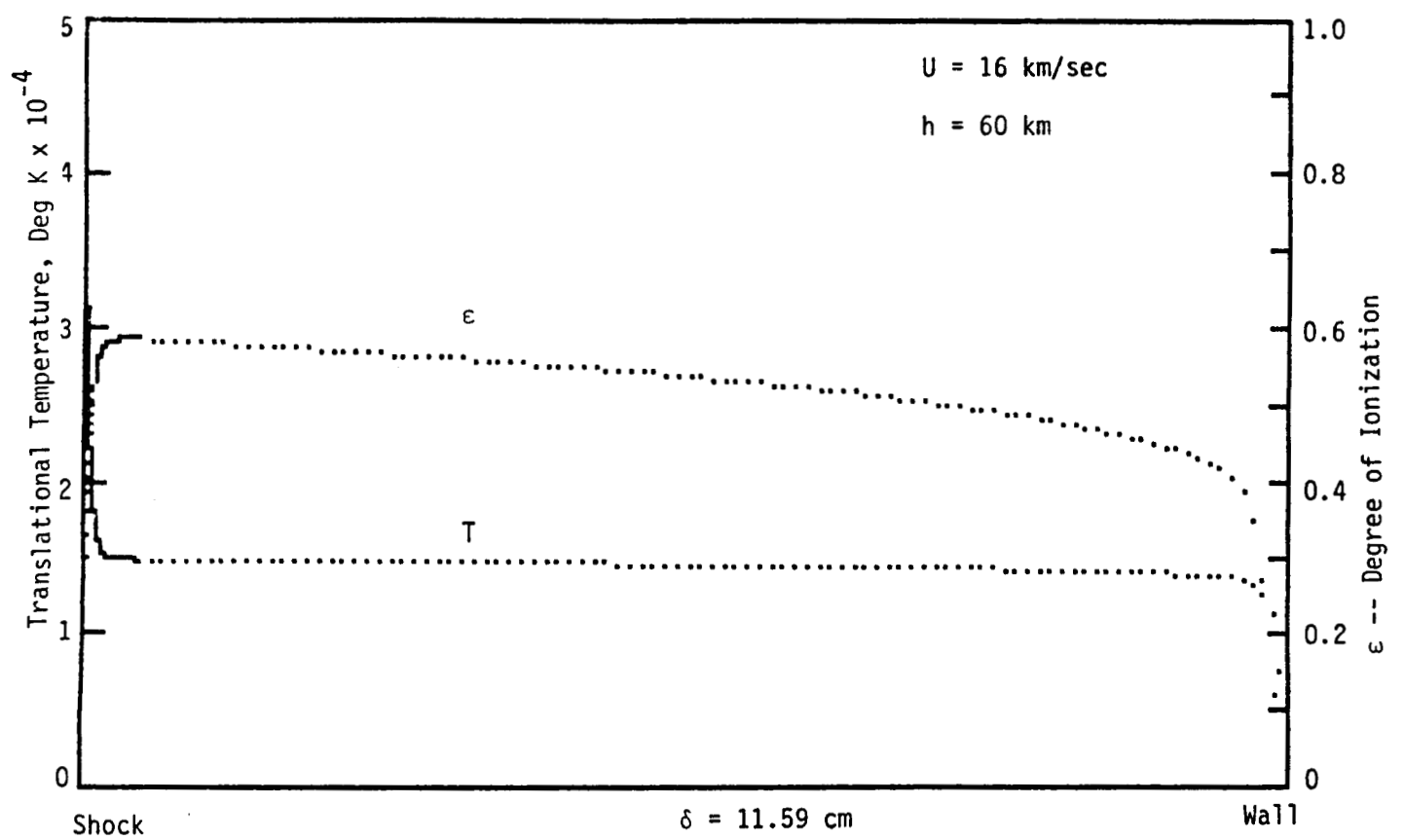


Figure 1(a) -- Stagnation Region Temperature and Ionization Profiles for an Altitude of 60 km.

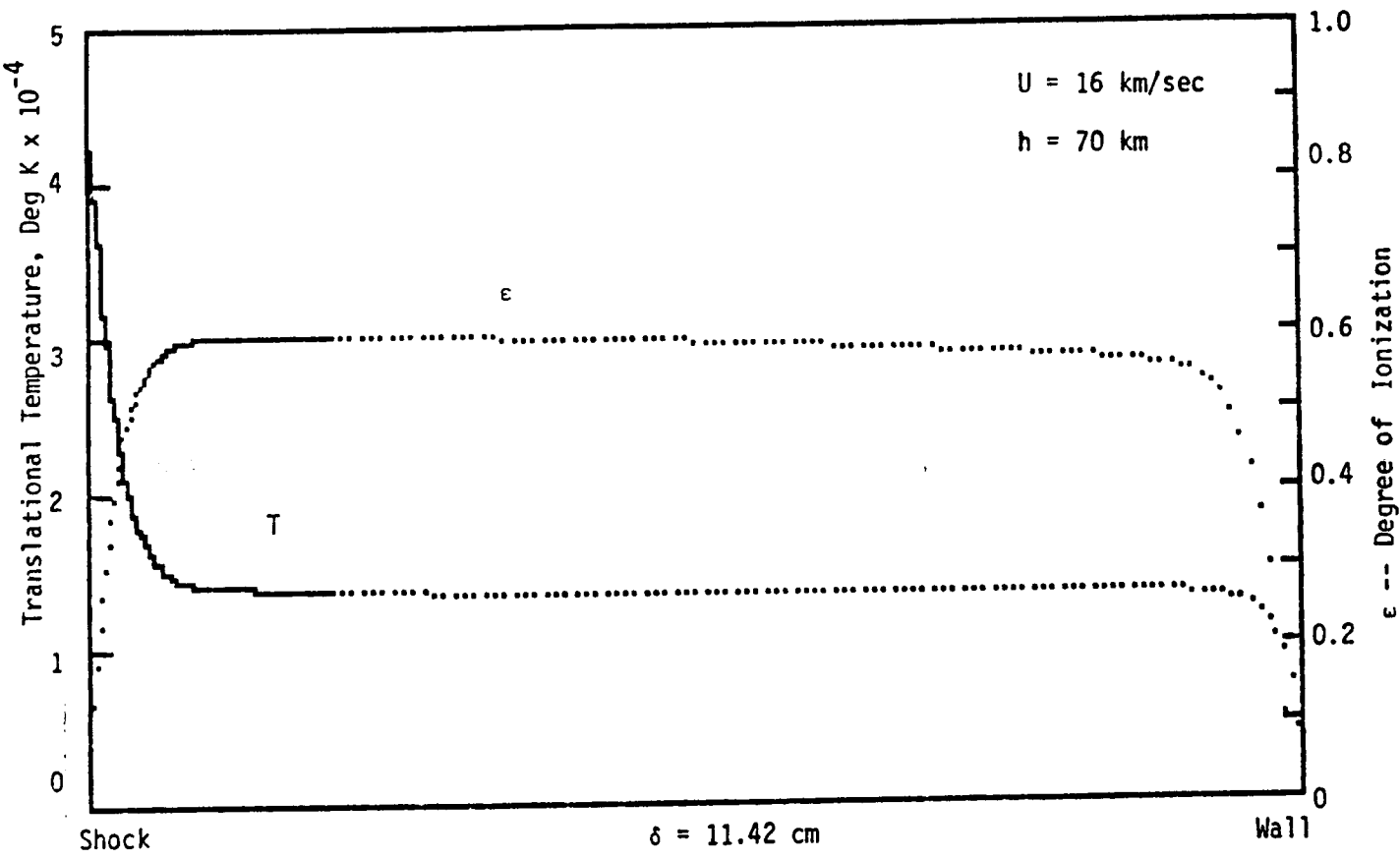


Figure 1(b) -- Stagnation Region Temperature and Ionization Profiles for an Altitude of 70 km.

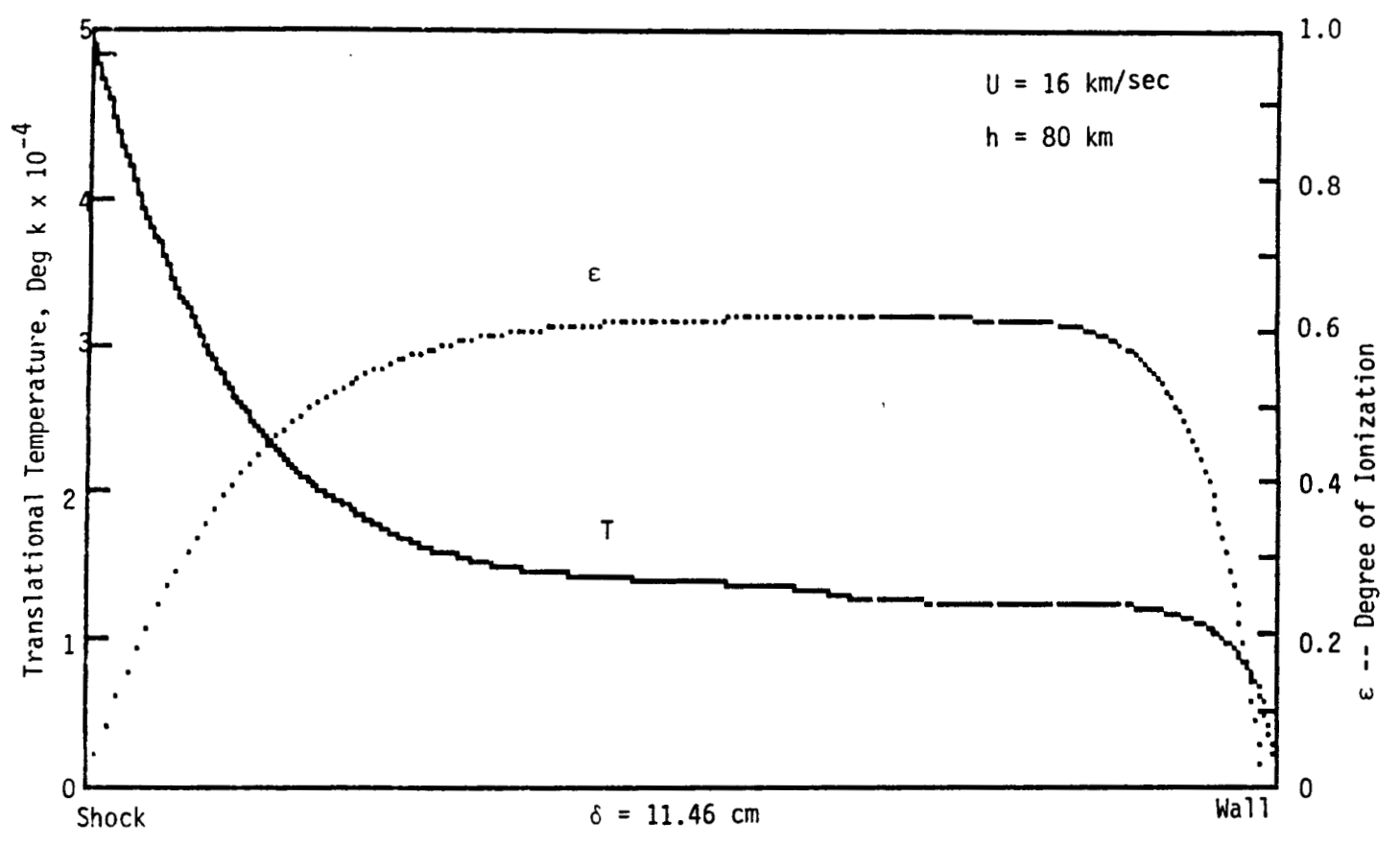


Figure 1(c) --  
Stagnation Region Temperature and Ionization Profiles  
for An Altitude of 80 km

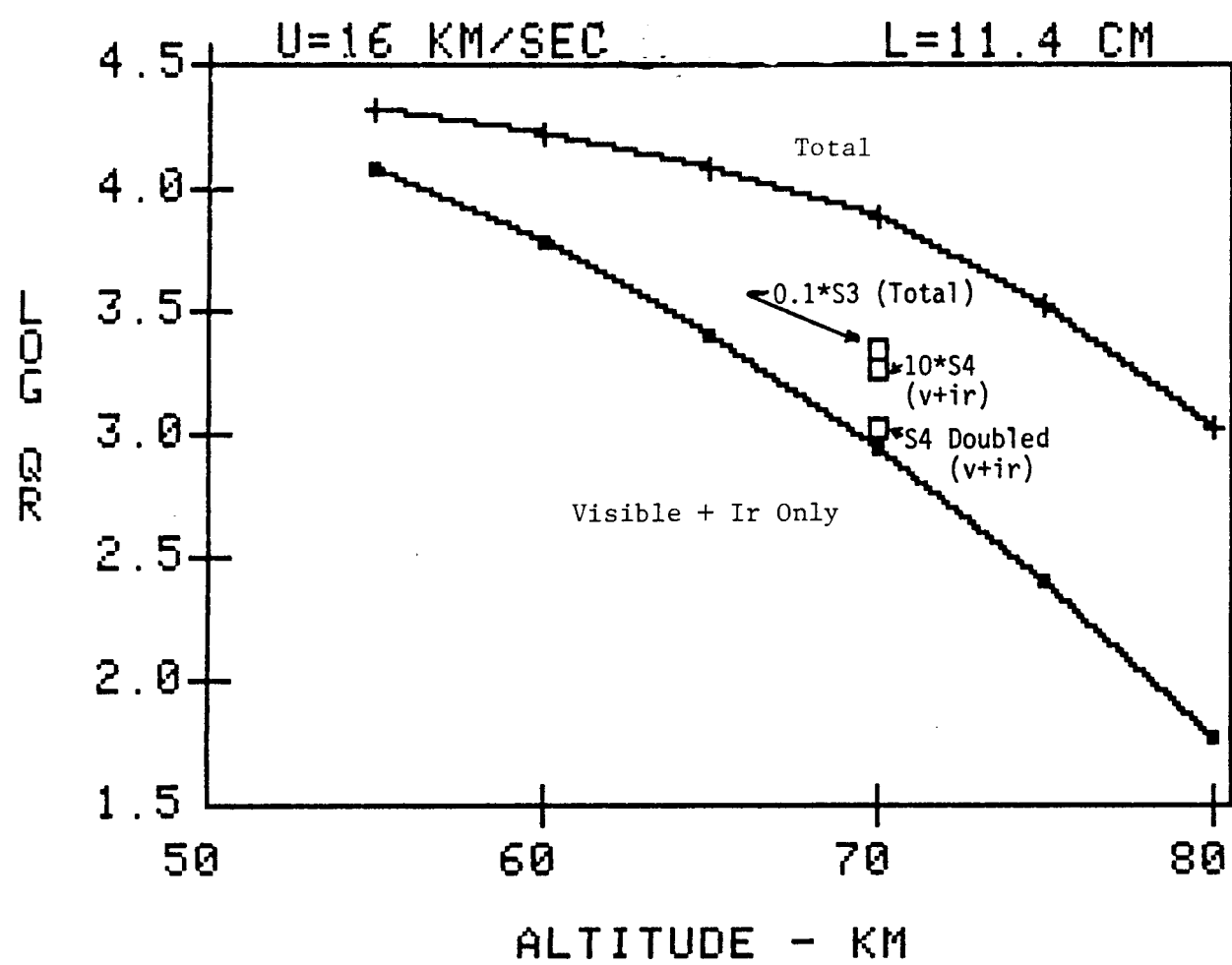


Figure 2 -- Radiative Heat Transfer Versus Altitude

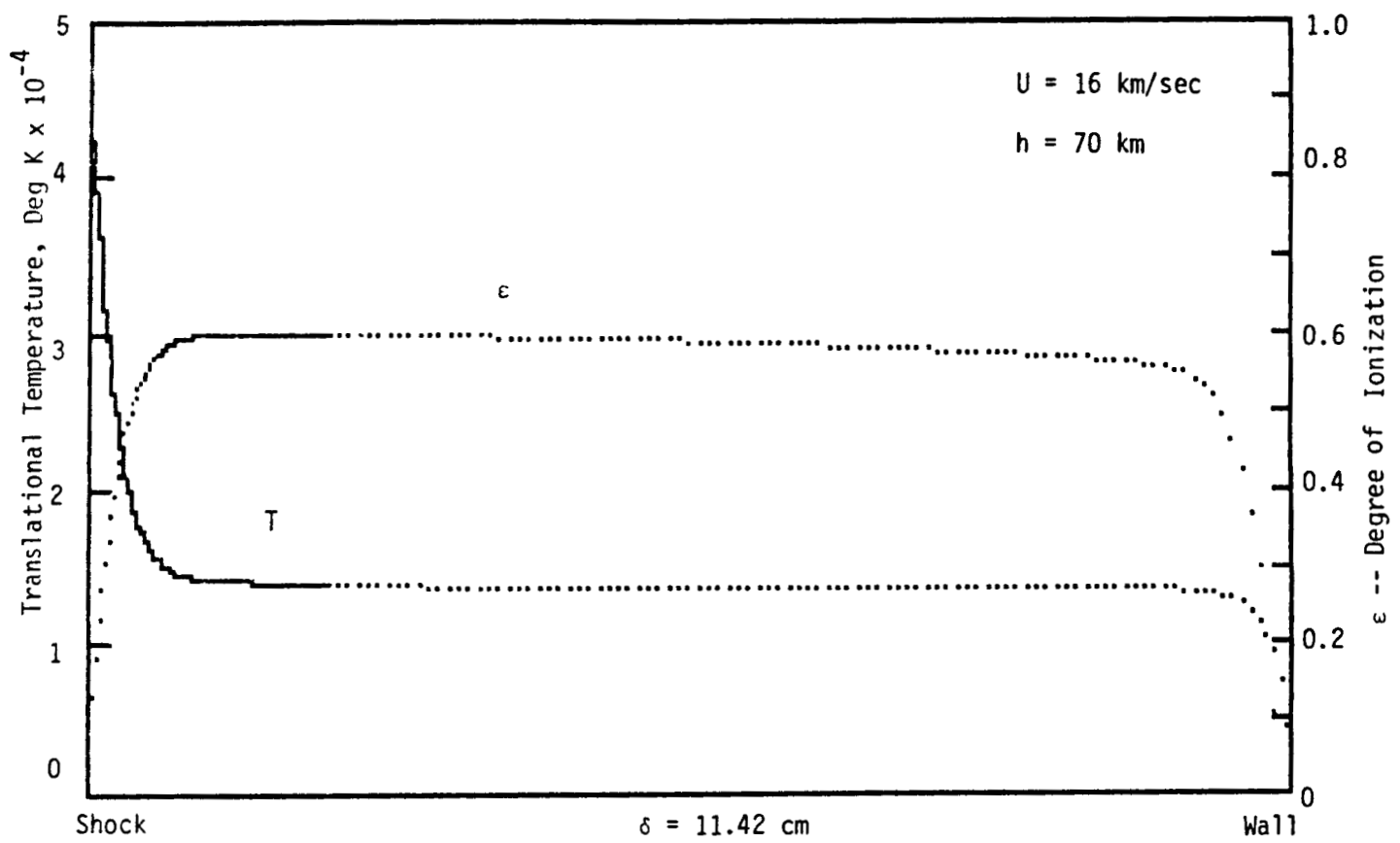


Figure 3 (a) -- Stagnation Region Temperature and Ionization Profiles for Shock Detachment Distance of 11.42 cm.

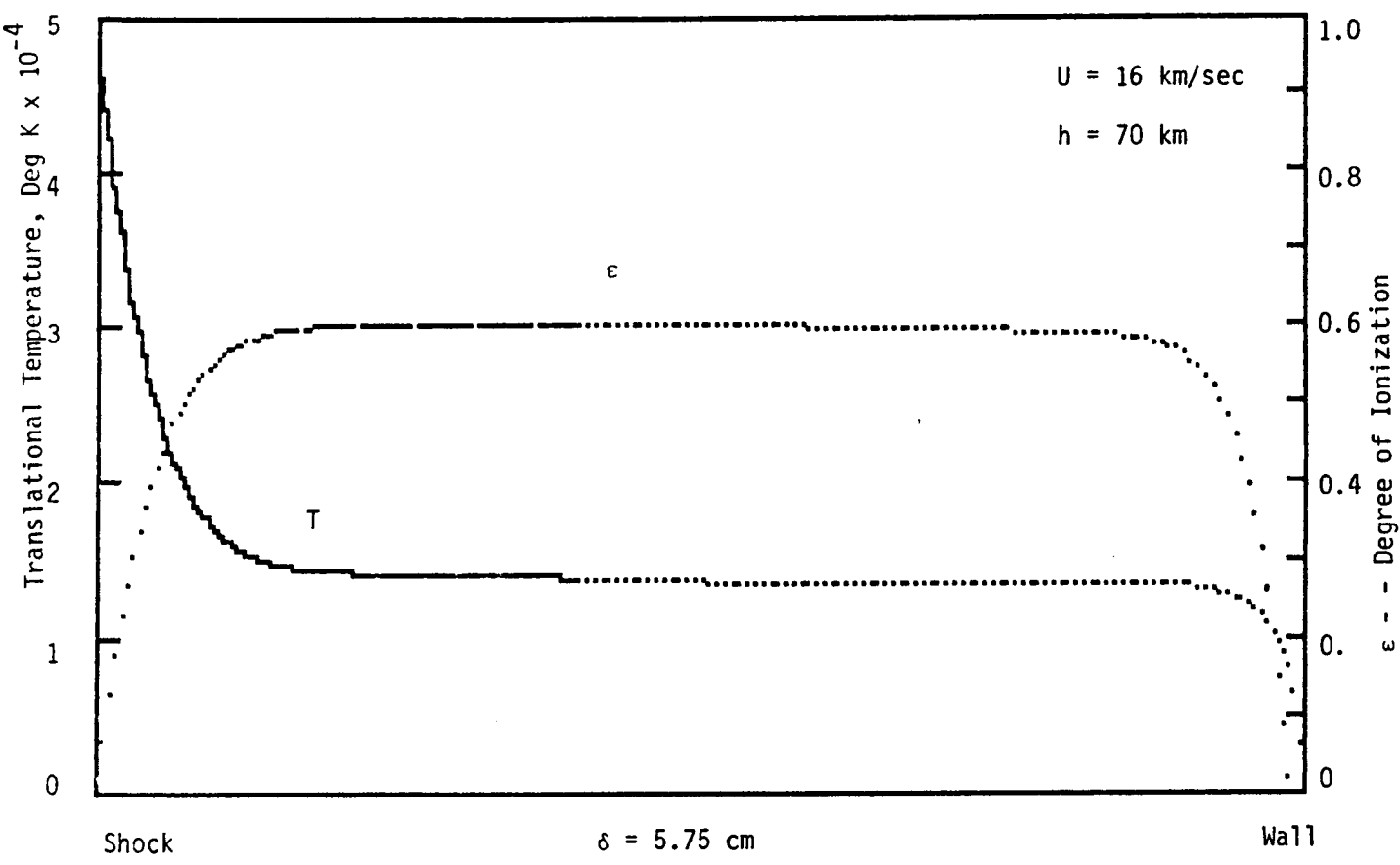


Figure 3 (b) -- Stagnation REgion Temperature and Ionization Profiles for Shock Detachment Distance of 5.75 cm.

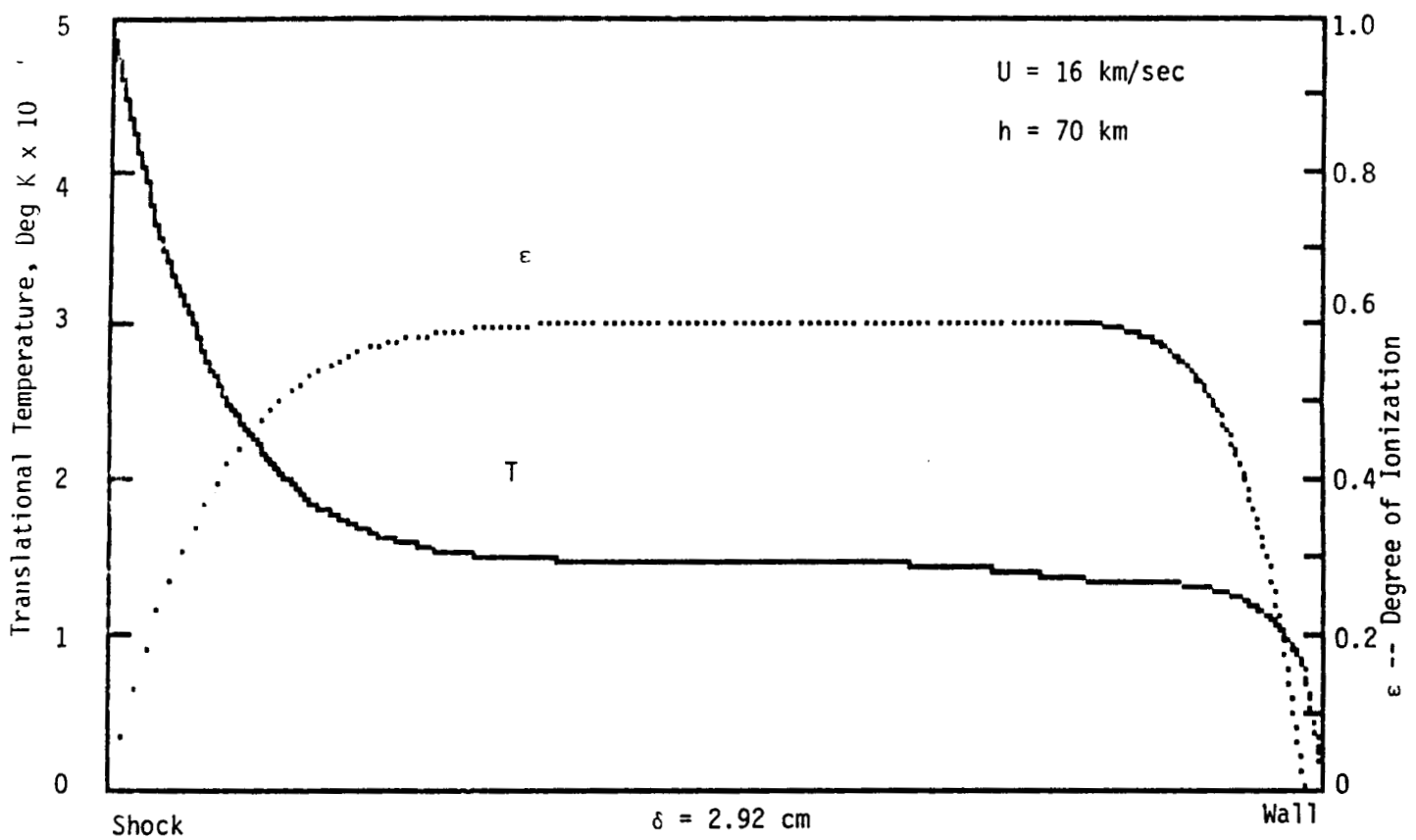


Figure 3 (c) -- Stagnation Region Temperature and Ionization Profiles for Shock Detachment Distance of 2.92 cm.

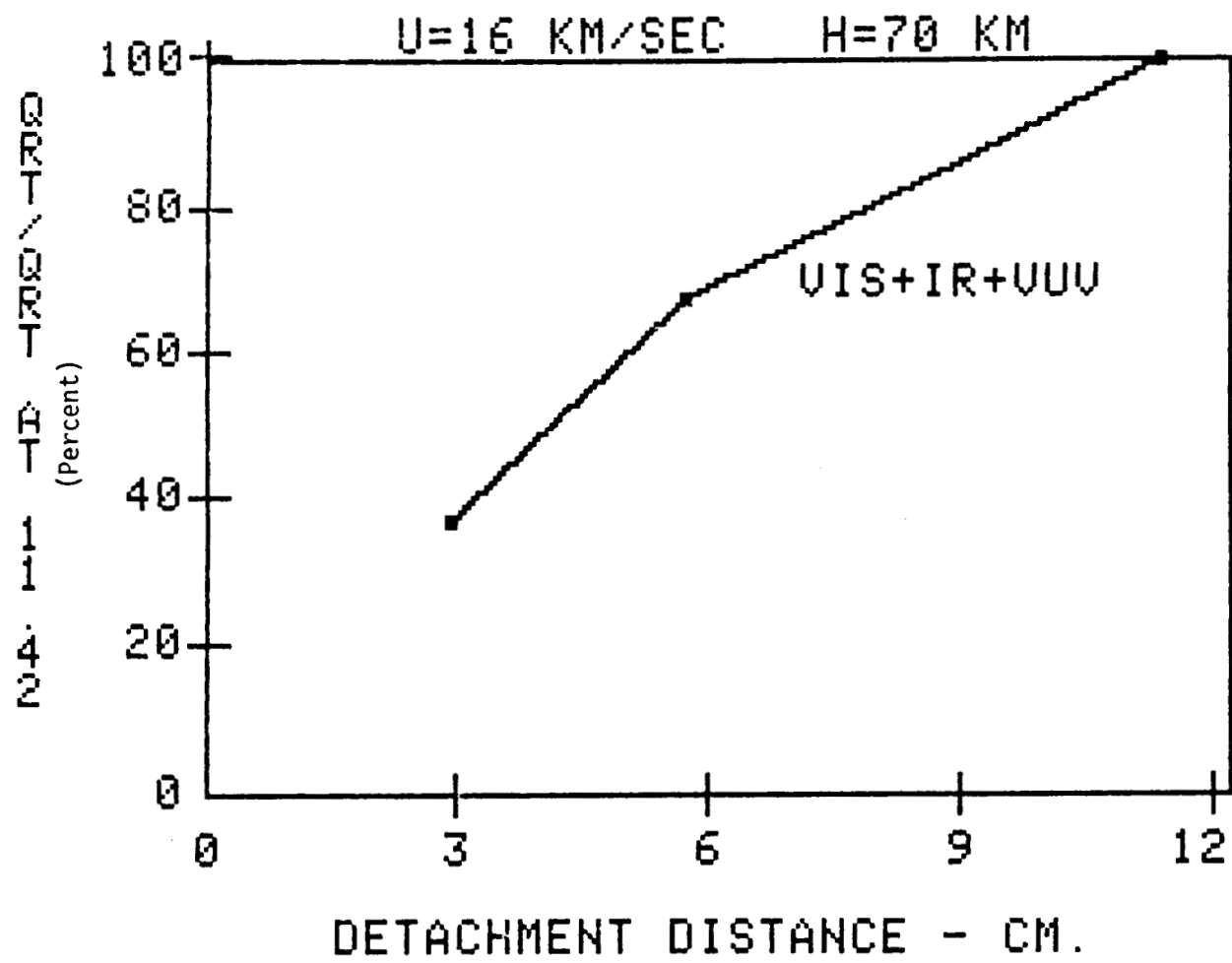


Figure 4 (a) -- Variation in Stagnation Point Radiative Heat Transfer with Shock Detachment Distance (Total)

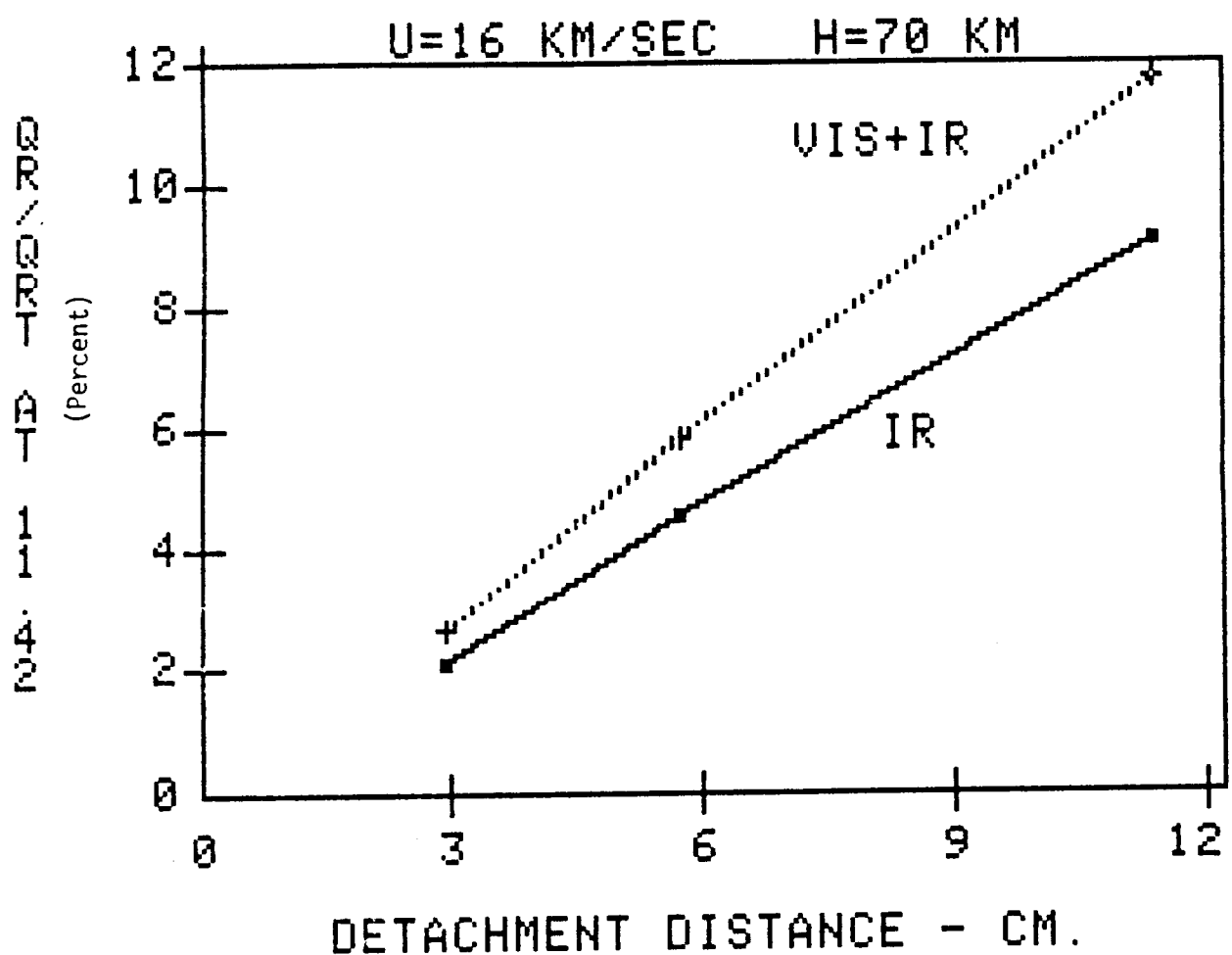


Figure 4 (b) -- Variation in Stagnation Point Radiative Heat Transfer with Shock Detachment Distance  
(Visible and Infrared Contributions Only)

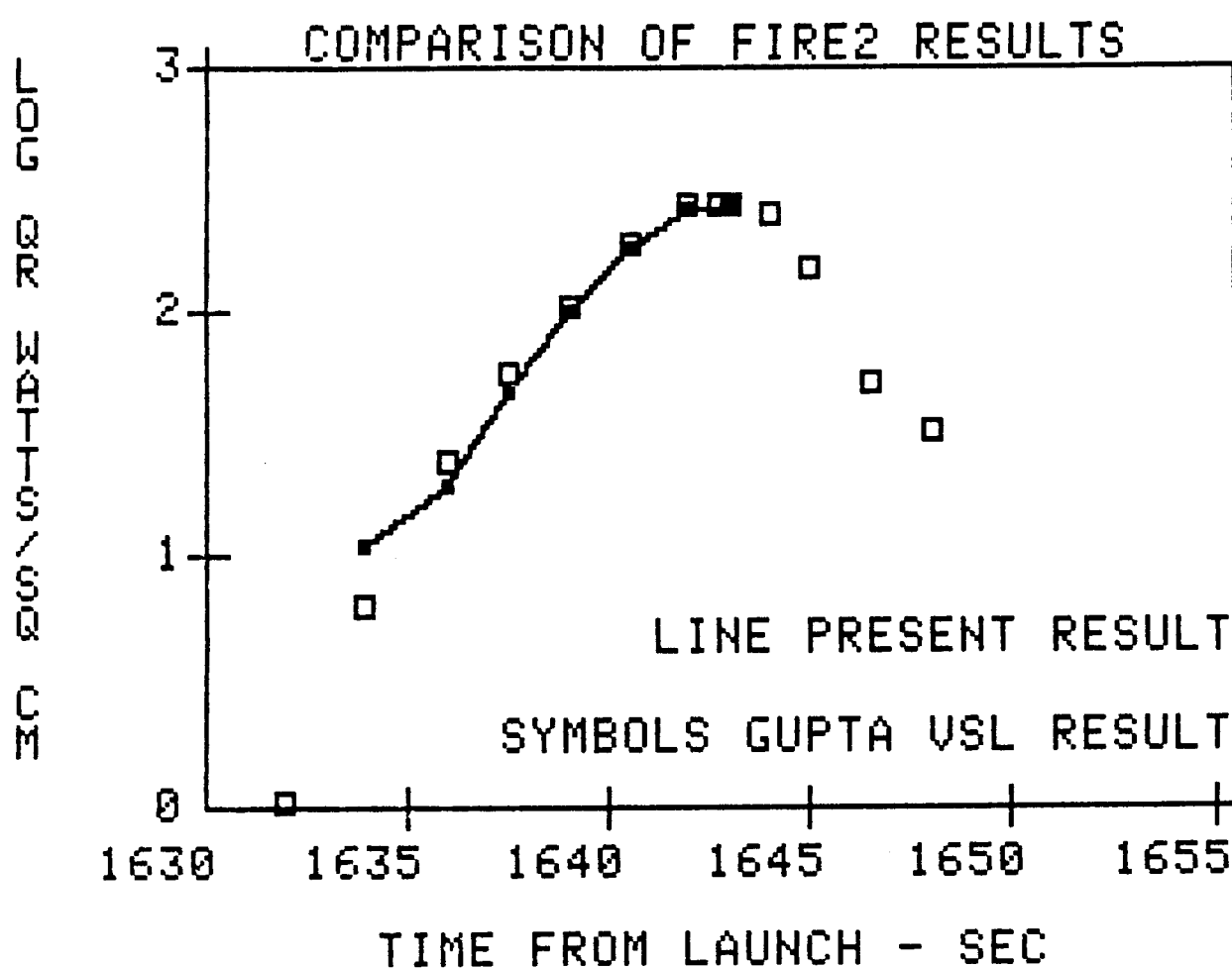


Figure 5 -- Comparison of Present Approximate Results  
with Equilibrium Viscous Shock Layer Results  
of Gupta (Visible plus Infrared Contribution Only)

## APPENDIX II

Comparison of Vibration Dissociation Coupling and Radiative Heat Transfer  
Models for AOTV/AFE Flowfields

COMPARISON OF VIBRATION DISSOCIATION COUPLING AND RADIATIVE HEAT  
TRANSFER MODELS FOR AOTV/AFE FLOWFIELDS

Leland A. Carlson\*, Glenn Bobskill\*\*, and Robert Greendyke\*\*  
Texas A&M University  
College Station, Texas 77843-3141  
(409)-845-1426

(Submitted for Presentation at the AIAA Thermophysics, Plasmadynamics,  
and Lasers Conference, June 27-29, 1988, San Antonio, Texas)

EXTENDED ABSTRACT

Introduction

In the future aero-assisted orbital transfer vehicles (AOTVs) will be used to operate, supply, maintain, and man satellites and space stations and to return from lunar and Mars missions. Those vehicles descending from geosynchronous to high or low earth orbit will operate in the entry and aero-assisted mode at velocities ranging from 7 to 11 km/sec at altitudes of 70 to 100 Km., with a nominal entry velocity of 10 km/sec and peak dynamic pressure occurring at 75 Km. Likewise, AOTVs returning from the Moon or Mars will enter at higher nominal velocities, 11 km/sec for lunar return and 13.5 to 16 km/sec for Martian return; and, thus, they will have a wider operating range from 7 to 18 km/sec at 60 to 100 km.

Obviously, in order to efficiently design and operate such vehicles not only must the important factors affecting the vehicle flowfields be understood but also methods for rapidly predicting them must be available. While the corner and afterbody flows for such vehicles are complicated and highly rotational and viscous, the forebody flow structure thru much of the entry flight profile is dominated by nonequilibrium chemistry and radiation; and these phenomena may significantly affect the heat transfer to and perhaps the aerodynamics of the vehicle.

In many cases, detailed three dimensional nonequilibrium viscous computations of AOTV flowfields will be required in order to obtain complete understanding of various phenomena or to finalize a design. Such detailed computations, typically using the Navier-Stokes equations (Ref. 1), are extremely lengthy often requiring many hours of supercomputer time. In addition, while some of these methods include nonequilibrium chemistry, few include the effects of such nonequilibrium phenomena as vibration dissociation coupling and electron thermal

\* Professor of Aerospace Engineering, Associate Fellow AIAA

\*\* Graduate Research Assistant

nonequilibrium; and because of their lengthy computational times, these detailed methods are unwieldy for evaluating or developing models and approximations representing these nonequilibrium phenomena. Further, only a few have attempted to include radiative heat transfer (Ref. 2).

This paper will discuss one portion of an initial effort to evaluate and develop models and approximations for nonequilibrium chemical and radiating flows associated with AOTVs returning from orbital, lunar, and Martian missions and will be applicable to entry velocities ranging nominally from 7 Km/sec to 10 Km/sec. (Reference 3 will present results associated with the 10.5 to 18 Km/sec regime.) The objectives of this initial phase of the effort are to investigate and compare various vibration dissociation chemistry coupling models and radiative heat transfer approximations and determine the similarities, differences, and consequences of using these models in the AOTV flight regime.

### Approach

As indicated above, in order to investigate various vibration dissociation coupling and radiative heat transfer models efficiently, the use of a rapid flowfield solver is essential. After considering various possibilities, it was decided to use an inviscid nonequilibrium chemistry axisymmetric inverse method (Ref. 4) as the basic Euler equation flow solver. This method has been modified and extended to include as options various vibration dissociation coupling, shock jump, radiative heat transfer, and electron temperature models. Since this method can be easily used on a micro or mini-computer, it is computationally efficient; and it permits the study of user selected individual streamlines when the entire flowfield is not needed. In addition, as shown on Figure 1, this method can adequately model the forward face of the aero-assisted flight vehicle (AFE) as a 60 degree axisymmetric blunted cone.

Currently, this method is being used to study and evaluate five vibration dissociation chemistry coupling models -- vibrational equilibrium, coupled vibration dissociation (CVD) which includes vibrational nonequilibrium and its effect on dissociation, coupled vibration dissociation vibration (CVDV) which additionally accounts for the effect of dissociation on vibrational energy, CVDV Preferential which assigns a higher probability of dissociation to higher vibrational energy levels, and a Chul Park like model. The latter is similar to CVDV but uses a modified collisional term and a different form for the vibrational relaxation time correlation. These models are discussed in detail in References 2 and 5.

The inverse method is also being used to evaluate, and if necessary develop, various electron temperature models. In this context, the pharse electron temperature refers to a temperature representing both the bound electronic temperature and the characteristic temperature of the free electrons. In the nonequilibrium flow associated with the

front face of an AOTV/AFE vehicle, it is anticipated that over much of the nonequilibrium portion the electron temperature will be different and lower than the local heavy particle or translational temperature.

Among those models being considered is one in which the electron excitation is initially dominated by atom-molecule collisions after which the electron temperature is controlled by vibrational-electronic coupling (Ref. 6). It is anticipated that this specific model should be most applicable to the lower velocity and temperature regime near the end of the AOTV entry, although similar models may have a wider range of applicability. Others being investigated are equating the electron temperature to the local nitrogen vibrational temperature, under the assumption of strong vibration-electronic coupling, or letting the electron temperature be some constant value or the translational temperature, whichever is lower. The latter approximation is based upon the results of detailed studies for monoatomic gases (Ref. 7) and for nitrogen (Ref. 8) in which the electron temperature was computed using a separate but highly coupled and detailed energy equation.

In the area of radiation, several different models have been incorporated into the inverse approach and are being used to compute under the tangent slab approximation the radiative heat transfer to the model AFE vehicle in Figure 1. The "simplest" of these is an optically thin radiance model (Ref. 9) which accounts for thirteen different phenomena including molecular bands, nitrogen and oxygen free-bound and bound-bound processes, and various free-free phenomena. In addition, three different non-gray gas step models, which account for the effects of self-absorption in the computation of the heat transfer, are being investigated. (It should be noted that for the 7-10 km/sec AOTV regime self-absorption effects may be important in the body heat transfer, but the total radiative losses should be too small to induce any significant gasdynamic coupling.) Two of these models, a two step (Ref. 10) and a five step (Ref. 11) model are based on high temperature nitrogen and should be representative of high temperature air at temperatures above eight to ten thousand degrees Kelvin. The third model, however, uses eight steps (Ref. 12), was developed for high temperature air, and includes both atomic and molecular emission-absorption. Each of these models can be used with the various different electron temperature models and initially assumes that nonequilibrium effects can be approximated by using the local electron temperature and local species concentrations. This approach is conservative in that its usage should predict higher radiative heat transfer levels than would actually occur (Ref. 3). The effect of using correction factors for nonequilibrium effects on the source functions and absorption coefficients will be included in the final paper.

### Preliminary Results

In this section some preliminary results will be presented and discussed. All of these results were obtained using a 7 species ( $N_2$ ,  $O_2$ , N, O,  $NO$ ,  $NO+$ , and e) 6 reaction chemistry model. Results for the final paper will also include  $N_2^+$ ,  $N^+$ , and  $O^+$  and at least four additional reactions.

Figure 2 shows the body, shock, and some typical streamlines in the stagnation region. Most of the flowfield profiles which follow will be for the streamline marked  $XS=1.5$ , which crosses the bow shock 1.5 cm above the centerline; and these preliminary profiles will be plotted versus X, which is the coordinate along the shock wave. The correspondence between X values and locations on the streamline are noted on Figure 2.

Figures 3(a) and (b) compare temperatures obtained with the CVDV vibration dissociation coupling model with those obtained assuming vibrational equilibrium for conditions near the end of an AOTV entry. (Here  $TV$  represents the  $N_2$  vibrational temperature.) While the translational temperature in the vibrational equilibrium case decreases faster as expected, it is interesting to note that the electron temperature is almost identical in both cases. In addition, for the conditions shown, the electron temperature is considerably different than the nitrogen vibrational temperature. Thus, for this situation, it would probably be inappropriate to compute radiative heat transfer using the CVDV predicted nitrogen vibrational temperature as the electron temperature.

Figure 4 shows T and  $TV(N_2)$  profiles for a trajectory condition near the beginning of the entry, 10 Km/sec at 80 Km., again using the CVDV model. Note that for this case and model that the nitrogen vibrational temperature peaks at over 20,000 deg. K very close to the shock front. Also, while not shown, comparison of these results with those obtained assuming vibrational equilibrium indicate that the translational temperature profiles for the two models are almost identical except very close to the shock front.

However, examination of the corresponding concentration profiles, Figures 5(a) and 5(b), show that the molecular nitrogen dissociation is strongly affected (i.e. slowed down) by vibrational nonequilibrium effects. Since the resultant radiative heat transfer will to a great extent depend upon the concentrations of  $N_2$  and N, these differences could significantly affect  $N_2$  band and N line and continuum radiation. (These effects will be discussed in the final paper.) In addition, the  $NO$ ,  $NO+$ , and e concentrations are significantly different between the two models. For example, the  $NO$  peak mass fraction value is 0.024 for the CVDV model and 0.0396 for the vibrational equilibrium case. These differences may significantly affect contributions from the  $NO$  Beta and Gamma radiation bands.

Some preliminary results have also been obtained using a model similar to that proposed by Park (Ref. 2). In these initial computations the modifications associated with the nitrogen vibrational relaxation time and the collisional term in the CVDV vibrational energy equation have been included. However, the dissociation reactions are assumed to be controlled by the translational temperature rather than an average temperature based upon the square root of the product of the translational and nitrogen vibrational temperatures. The latter will be incorporated into the model and reported on in the final paper. The resulting temperature profiles and the nitrogen concentration profiles are shown on Figures 6 and 7, again for the streamline which crosses the shock front at 1.5 cm above the centerline.

Comparison of these results with those shown on Figures 4 and 5 reveals several interesting features. First, as would be expected, the Park vibrational model results in a slower rate of nitrogen dissociation and, therefore, increases the size of the nonequilibrium zone. Consequently the translational temperature and N<sub>2</sub> concentrations are higher and the N concentrations are lower throughout the region shown than the corresponding CVDV results. The most interesting result, however, is the nitrogen vibrational temperature profile. For the Park like model the peak value of TV(N<sub>2</sub>) is 13,370 K while for the CVDV model it is considerably higher at 20,900 K. Further, the subsequent behavior of the vibrational temperatures is considerably different. In the CVDV case, TV(N<sub>2</sub>) takes on values in the vicinity of 11,000 K; while for the Park like model the values are near 8600 K. Since it has been postulated (Ref. 2 and 6) that the electron temperature can be approximated by the nitrogen vibrational temperature over much of the flowfield, these differences would lead to significantly different predictions for the magnitude of the radiative heat transfer.

In addition, it is interesting that the plateau level of the TV(N<sub>2</sub>) on Fig. 6 is close to the post-normal shock equilibrium value for these conditions. Detailed calculations of electron tempeature usually indicate that the electron temperature initially peaks and then maintains an essentially constant value ranging from near to fifteen percent above the ideal equilibrium value. Thus, the TV(N<sub>2</sub>) values on Fig. 6, while possibly low, may be closer to the actual TE values than the TV(N<sub>2</sub>) values shown on Fig. 4. This feature and the development of a model to take advantage of it are currently being investigated. Table I below lists some typical values for the CVDV and Park like models.

Preliminary radiative heat transfer results have also been obtained using three different radiation models and the CVDV vibration dissociation coupling model. These results have been computed as a function of body location using the tangent slab approximation, local species concentrations, and assuming that the electron temperature is equivalent to the CVDV nitrogen vibrational temperature. This latter assumption and the fact that the computations did not include any nonequilibrium correction factors on the source functions or absorption coefficients probably makes the present results conservative. (Results

with nonequilibrium correction factor approximations will be included in the final paper.)

In the interest of brevity in this abstract, preliminary results will only be presented for the body point located 9 cm above the centerline. Table II below presents results for three different radiation models by wavelength region, and Figures 8-10 show the radiative heat transfer spectrally. As can be seen from the tabular data, the total predicted values disagree by only a factor of two, which is quite surprising considering the differences in the models and the fact that none were originally developed for the present low density regime. In addition, all of the models predict that most of the radiative heat transfer originates from the ultra-violet. This trend is evident in Figure 8 for the non-absorbing radiance model, where most (93%) of the energy is in the region above 6 ev.

Figure 9 shows similar results for the five step absorbing model, which would be expected to yield lower total heat transfer due to absorption effects. Because of the self-absorption, very little radiative energy reaches the wall from the vacuum ultra-violet above 11 ev. However, this model predicts a considerable contribution from UV lines in the 7.88 - 9.55 ev range plus significant amounts from the visible (1.573-7.88 ev) continuum and IR lines (1.298-1.573 ev). It should be noted that this model is based upon nitrogen and does not include any oxygen or N<sub>2</sub>+(1-) emissions. However, it was for the visible and IR regions verified against experimental data at similar temperatures, although higher pressures.

Finally, Figure 10 presents the spectral variation for the eight step model absorption coefficient step model. (Only seven steps appear present. However, two steps are for the same region and have been combined on the plot and in the tables.) Like the other models, the majority of the radiative heating originates from the region above 6 ev., but it also predicts more heating from both the ultra-violet and the visible plus IR regions than the 5 step model. Possibly this difference is due to the fact that the 8 step model includes contributions due to oxygen, molecular band systems, and additional atomic lines in the 911- 1800 Å VUV region. (The five step model only includes VUV lines in the 1300-1570 Å region.) In particular, for the present conditions N<sub>2</sub>+(1-) may be significant, which would explain the large contribution in the 8 step model in the 3 - 5 ev region. These possibilities are under investigation and will be reported in the final paper.

Again it should be noted that these radiative heating results were based upon the CVDV results using TE=TV(N<sub>2</sub>) and with no nonequilibrium correction factors applied to the source functions or absorption coefficients. For the present highly nonequilibrium conditions, the latter could reduce the heating by as much as an order of magnitude (Ref. 3), and thus they will be included in results presented in the final paper. Also, the choice of electron temperature model will

significantly affect the radiative heating values. Thus, various models, including the Park like model, will be used to evaluate the radiative heat transfer and the results will be discussed. Also, the present results do not include any absorption effects due to the presence of a "cool" boundary layer on the surface of the vehicle. However, preliminary results of Ref. 3 indicate that this will only affect the far VUV.

#### Summary

An axisymmetric nonequilibrium inverse method has been modified and extended and used to investigate and compare various vibration dissociation chemistry coupling models and radiative heat transfer approximations. The similarities, differences, and consequences of using these models in the AOTV flight regime will be discussed.

#### Acknowledgement

This effort was primarily supported under a subportion of NASA Grant No. NAG 9-192 from the NASA Johnson Space Center. The grant monitor is Dr. Winston Goodrich, Aerosciences Branch.

#### References

1. Gnoffo, P. and Greene, F. A., "A Computational Study of the Flowfield Surrounding the Aeroassist Flight Experiment Vehicle," AIAA Paper No. 87-1575, June 1987.
2. Park, C., "Assessment of Two-Tempeature Kinetic Model for Ionizing Air," AIAA Paper No. 87-1574, June 1987.
3. Carlson, L. A., "Approximations for Hypervelocity Nonequilibrium Radiating, Reacting, and Conducting Stagnation Regions," Submitted for presentation at the AIAA Thermophysics, Plasmadynamics, and Lasers Conference, June 1988.
4. Grosse, W. L., "A Thin Shock Layer Solution for Nonequilibrium, Inviscid Hypersonic Flows in Earth, Martian, and Venusian Atmospheres," NASA TN D-6529, December 1971.
5. Marrone, P. V., "Inviscid, Nonequilibrium Flow Behind Bow and Normal Shock Waves, Part I. General Analysis and Numerical Examples," CAL Report No. QM-1626-A-12(I), Cornell Aeronautical Laboratory, Inc., Buffalo, N.Y., May 1963.
6. Carlson, L. A., "Electron Temperature and Relaxation Phenomena behind Shock Waves," Journal of Chemical Physics, Vol. 57, No. 2, July 1972, pp. 760-766.

7. Nelson, H. F. and Goulard, R., "Structure of Shock Waves with Nonequilibrium Radiation and Ionization," The Physics of Fluids, Vol. 12, No. 8, Aug. 1969, pp. 1605-1617.
8. Carlson, L. A., "Radiative Gasdynamic Coupling and Nonequilibrium Effects behind Reflected Shock Waves," AIAA Journal, Vol. 9, No. 5, May 1971, pp. 858-865.
9. Curtiss, J.T., and Strom, C. R., "Computations of the Nonequilibrium Flow of a Viscous, Radiating Fluid about a Blunt Axisymmetric Body," AFFDL-TR-67-40, Volume 1, June 1967.
10. Anderson, Jr., J.D., "Heat Transfer from a Viscous Nongray Radiating Shock Layer," AIAA Journal, Vol. 6, No. 8, Aug. 1968, pp. 1570-1573.
11. Knott, P. R., Carlson, L. A., and Nerem, R. M., "A Further Note on Shock Tube Measurements of End Wall Radiative Heat Transfer in Air," AIAA Journal, Vol. 7, No. 11, Nov. 1969, pp. 2170-2172.
12. Olstad, W. B., "Nongray Radiating Flow about Smooth Symmetric Bodies," AIAA Journal, Vol. 9, No. 1, January 1971, pp. 122-130.

Table I -- Comparison of CVDV and Park Like Models

CVDV				Park Like		
X	T	TV(N2)	C(N)	T	TV(N2)	C(N)
1.56	22780	20900	.2911	26840	13370	.1634
2.01	14950	12910	.6165	16940	9279	.5336
2.53	13640	11860	.6759	15050	8628	.6120
3.53	12840	11260	.7136	13780	8515	.6673
5.54	12350	10920	.7369	12900	8630	.7073
10.00	12090	10740	.7492	12310	8749	.7349

Note: X is coordinate parallel to shock. For corresponding flow location see Fig. 2. Above for streamline XS=1.5 .

Table II -- Radiative Heat Transfer

Model I -- Radiance Model -- No self-absorption	
Region	QR (watts/sq cm)
O2(S-R)	0.002
N2(1+ & 2+)	0.045
NO (Beta + Gamma)	0.043
NO(ir)	0.000
N(Free-free)	0.000
O(Free-free)	0.000
N(Free-bound,2000-5000)	217.5
N(500-2000)	4045
O(2000-5000)	169.9
O(500-2000)	1488
Total	5920

Model II - 5 Step Model based on nitrogen	
Wavelength Region	QR(watts/sq cm)
620 - 1100	98.2
1100 - 1300	171.3
1300 - 1570	3102
1570 - 7870	240.1
7870 - 9557	243.9
Total	3856

Model III - 8 Step Model based on air	
Wavelength Region	QR(watts/sq cm)
400 - 852	48.43
852 - 911	449.3
911 - 1020	1553
1020 - 1130	526.2
1130 - 1801	2809
1801 - 4000	1578
4000 -	937.8
	7901

Table III -- Comparison of Radiative Heating Models Above and Below  
Approximately 2000 A

Region	Model I	Model II	Model III
<2000	5533	3371.5	5385.93
>2000	387.4	484	2515.8

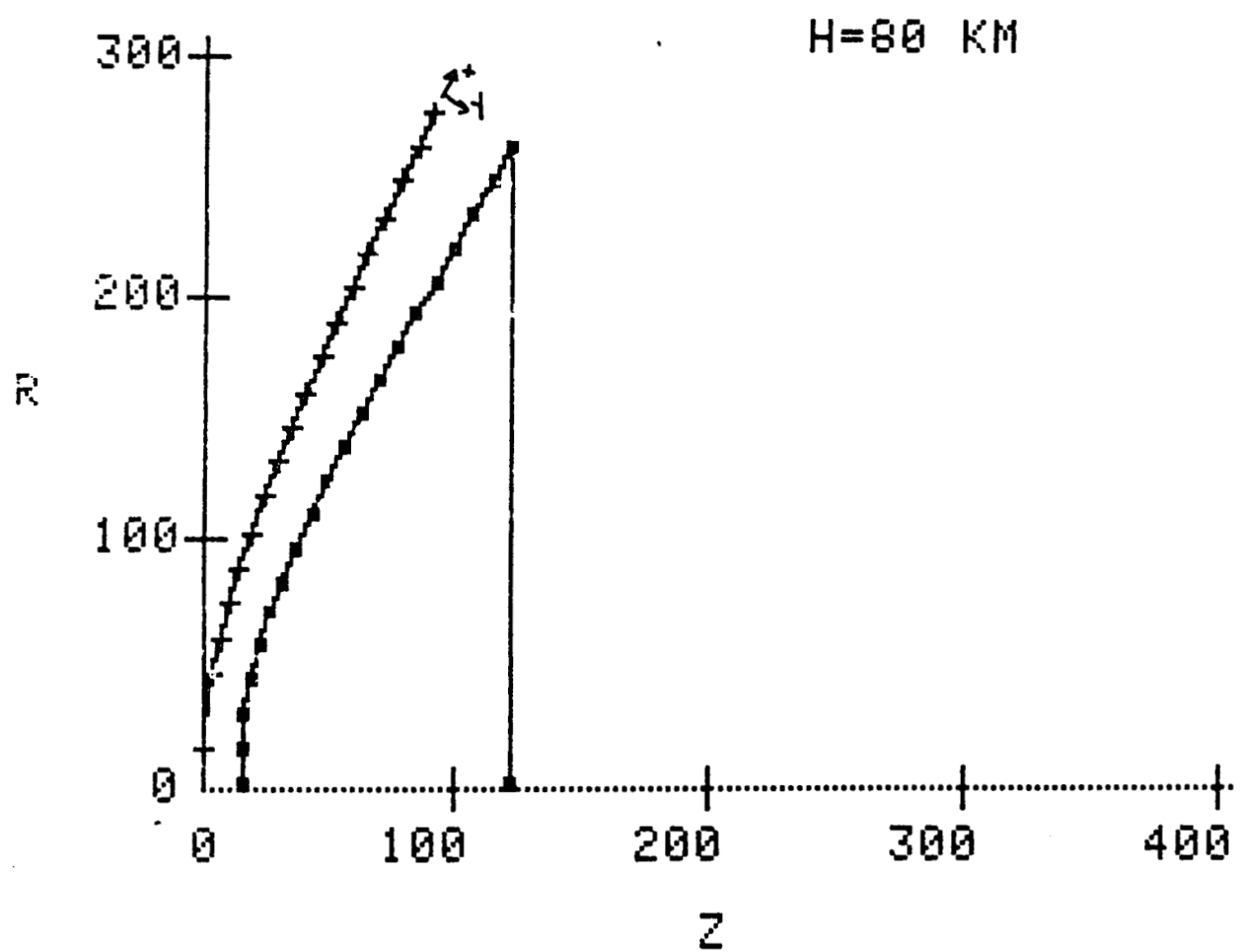


Figure 1 -- Shock Shape and  $60^{\circ}$  Blunt Cone Shape Generated  
by Inverse Code

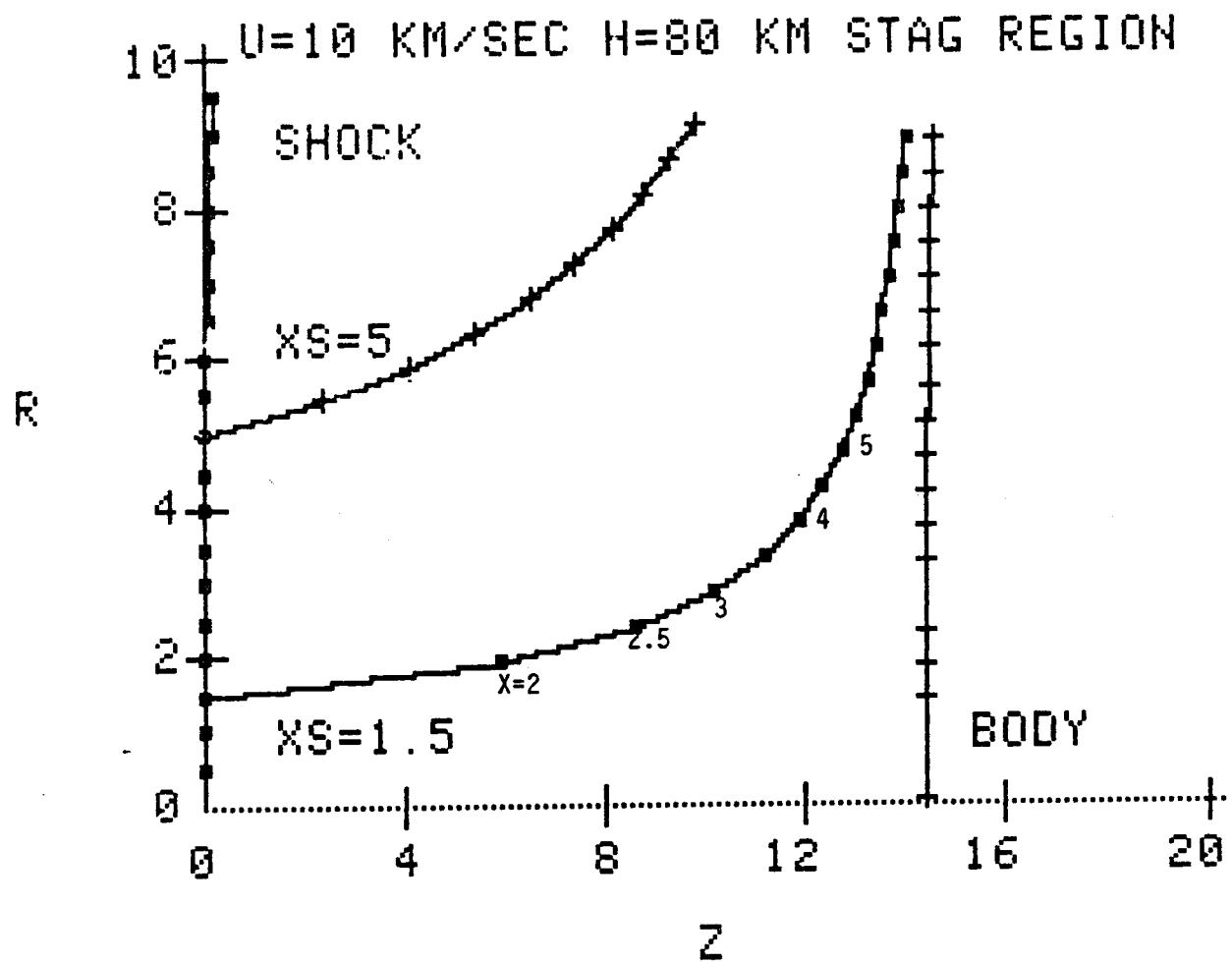


Figure 2 -- Typical Stagnation Region Streamlines

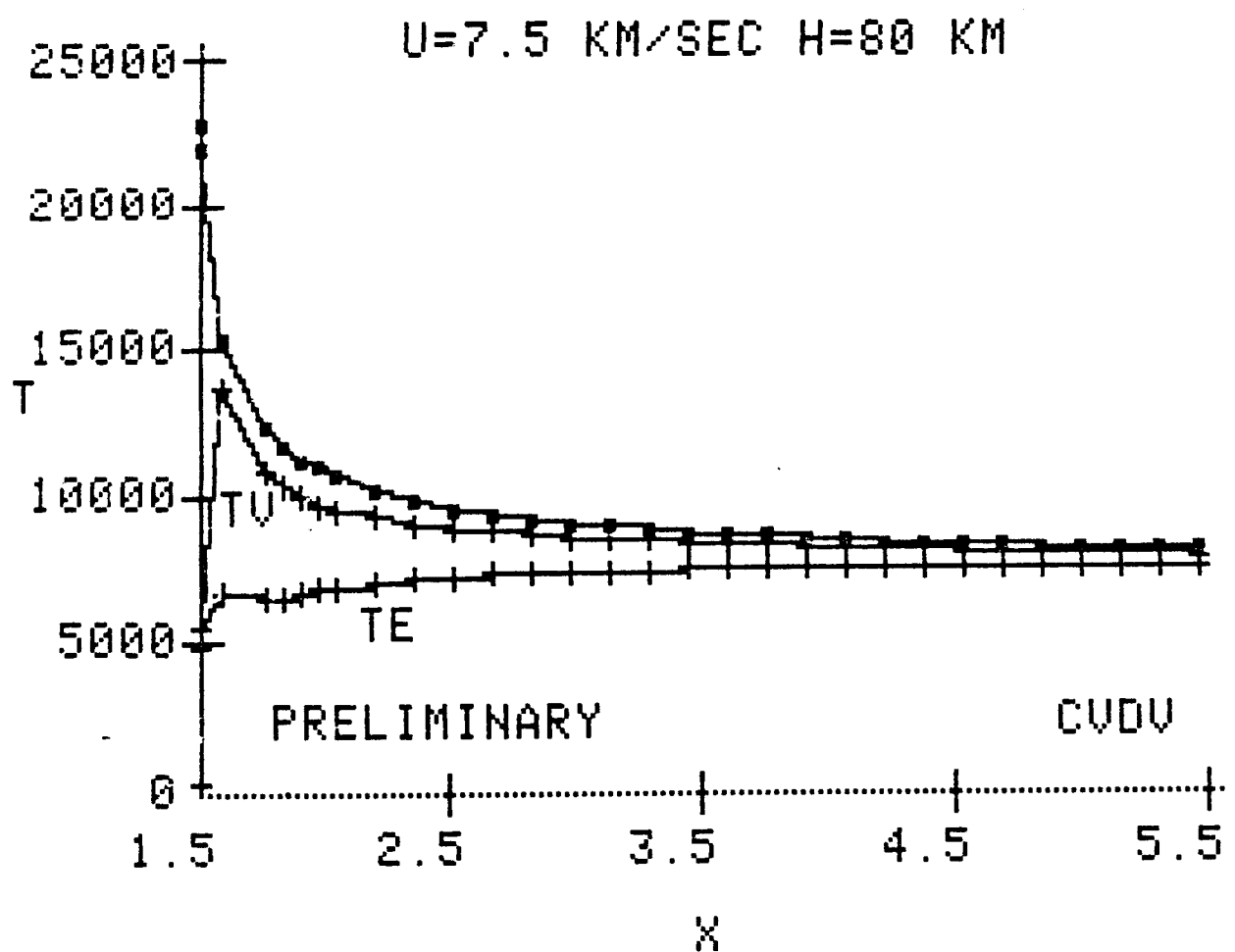


Figure 3(a) Translational, Nitrogen Vibrational, and Electron Temperature Profiles Along Streamline XS=1.5

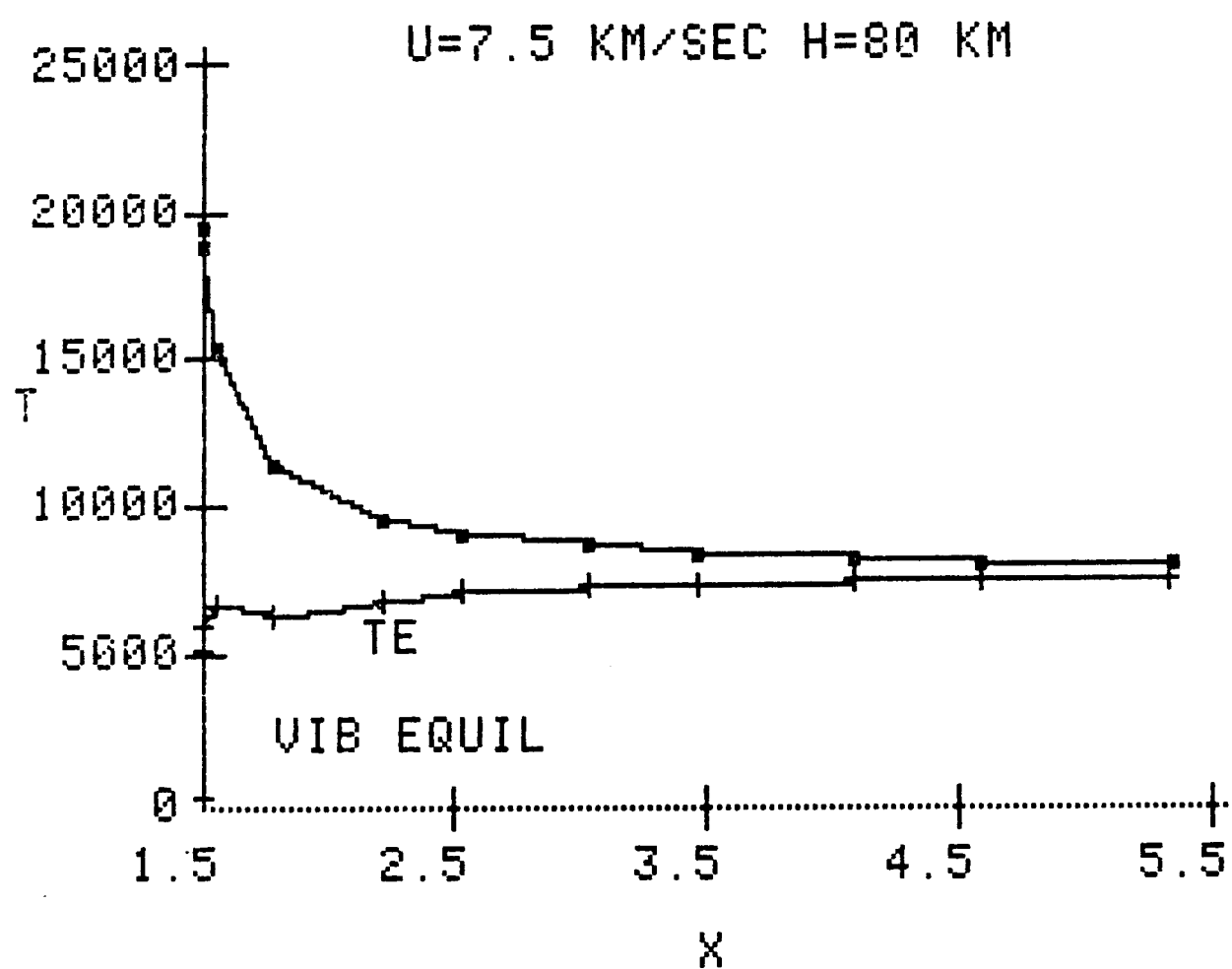


Figure 3(b) -- Translational and Electron Temperature Profiles  
Along Streamline XS=1.5 (Vibrational Equilibrium)

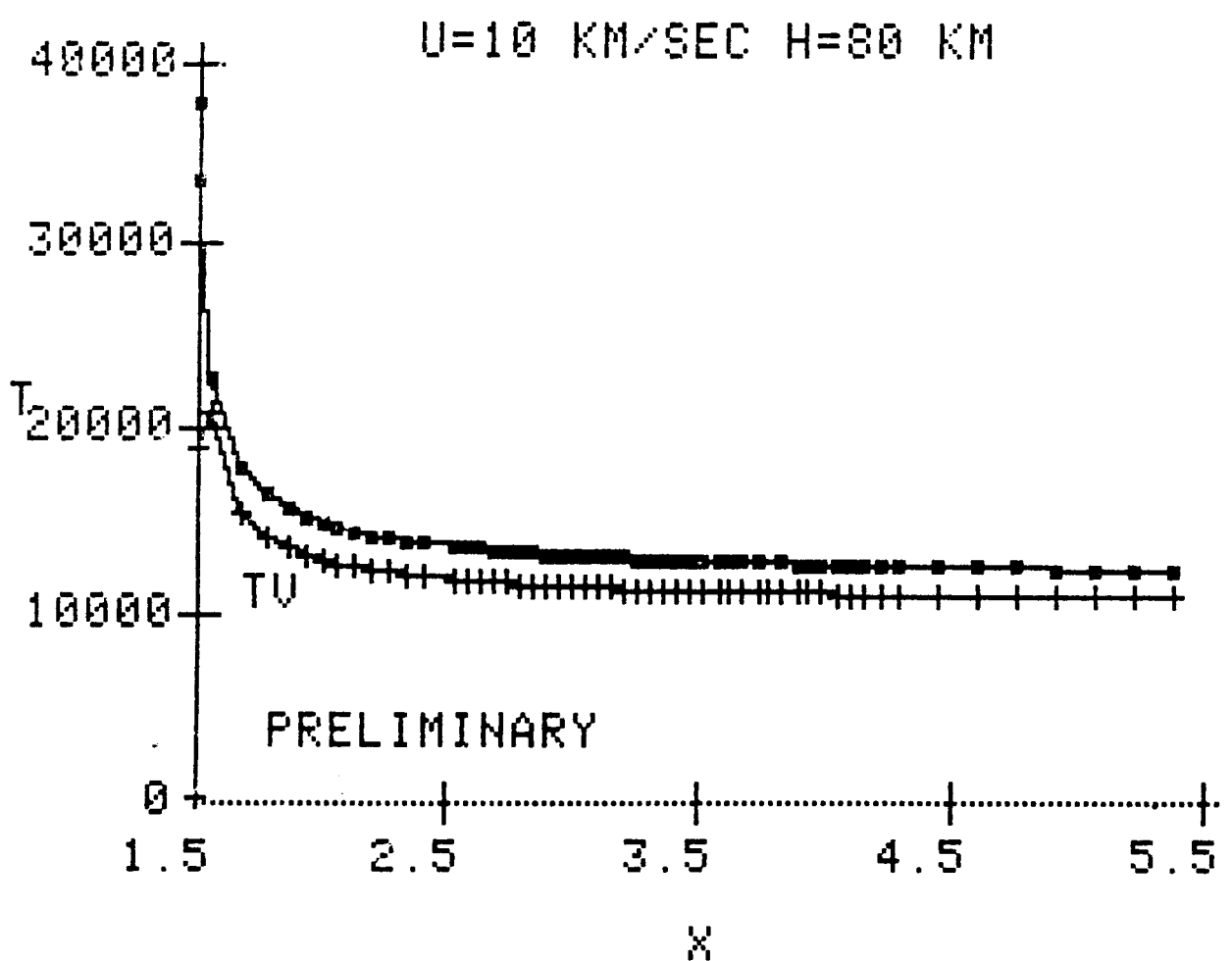


Figure 4 -- Temperature Profiles Along Streamline  $XS=1.5$   
(CVDV Vibration Dissociation Coupling Model)

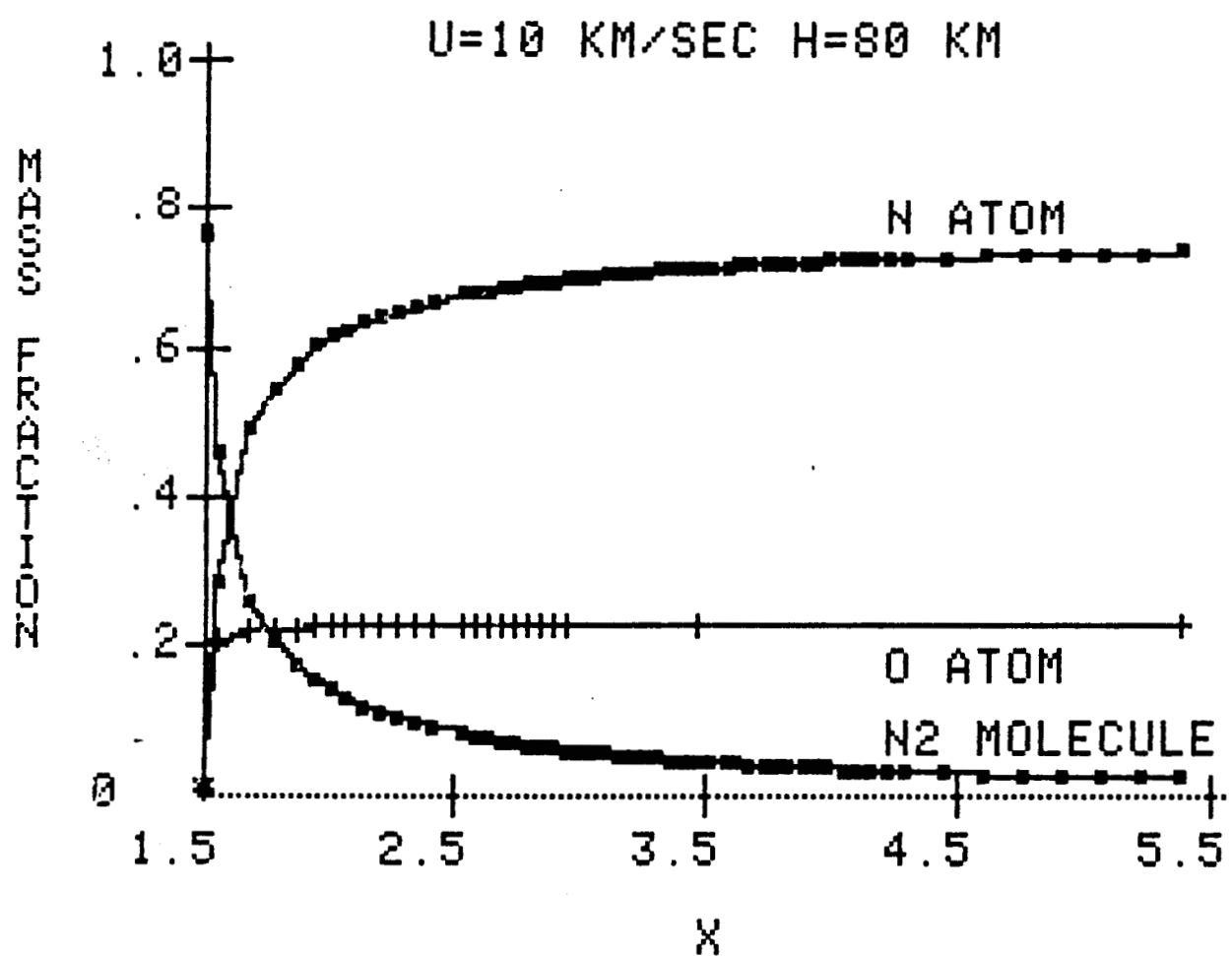


Figure 5(a) Concentration Profiles Along Streamline XS=1.5  
(CVDV Vibration Dissociation Coupling Model)

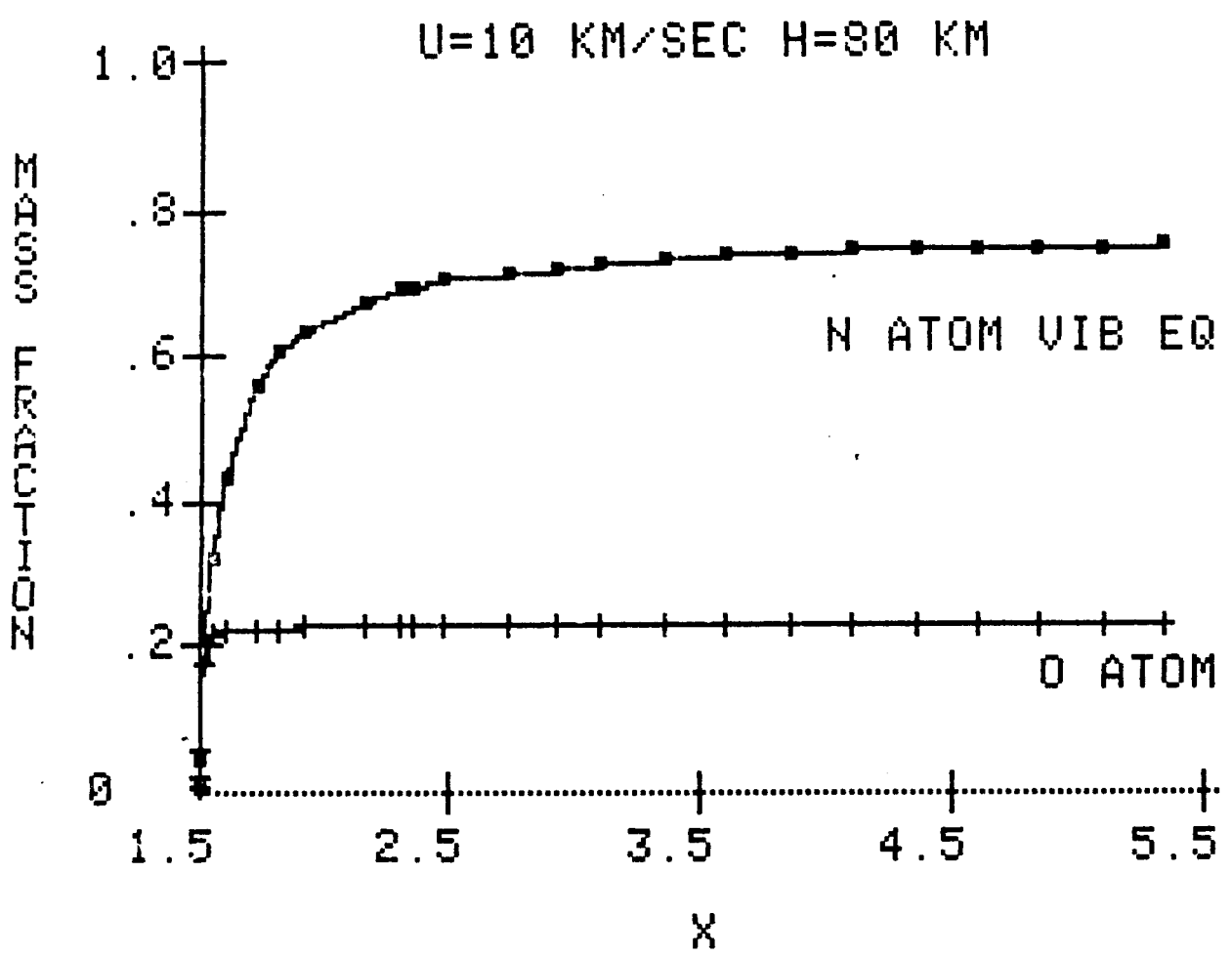


Figure 5(b) -- Concentration Profiles Along Streamline XS=1.5  
(Vibrational Equilibrium Case)

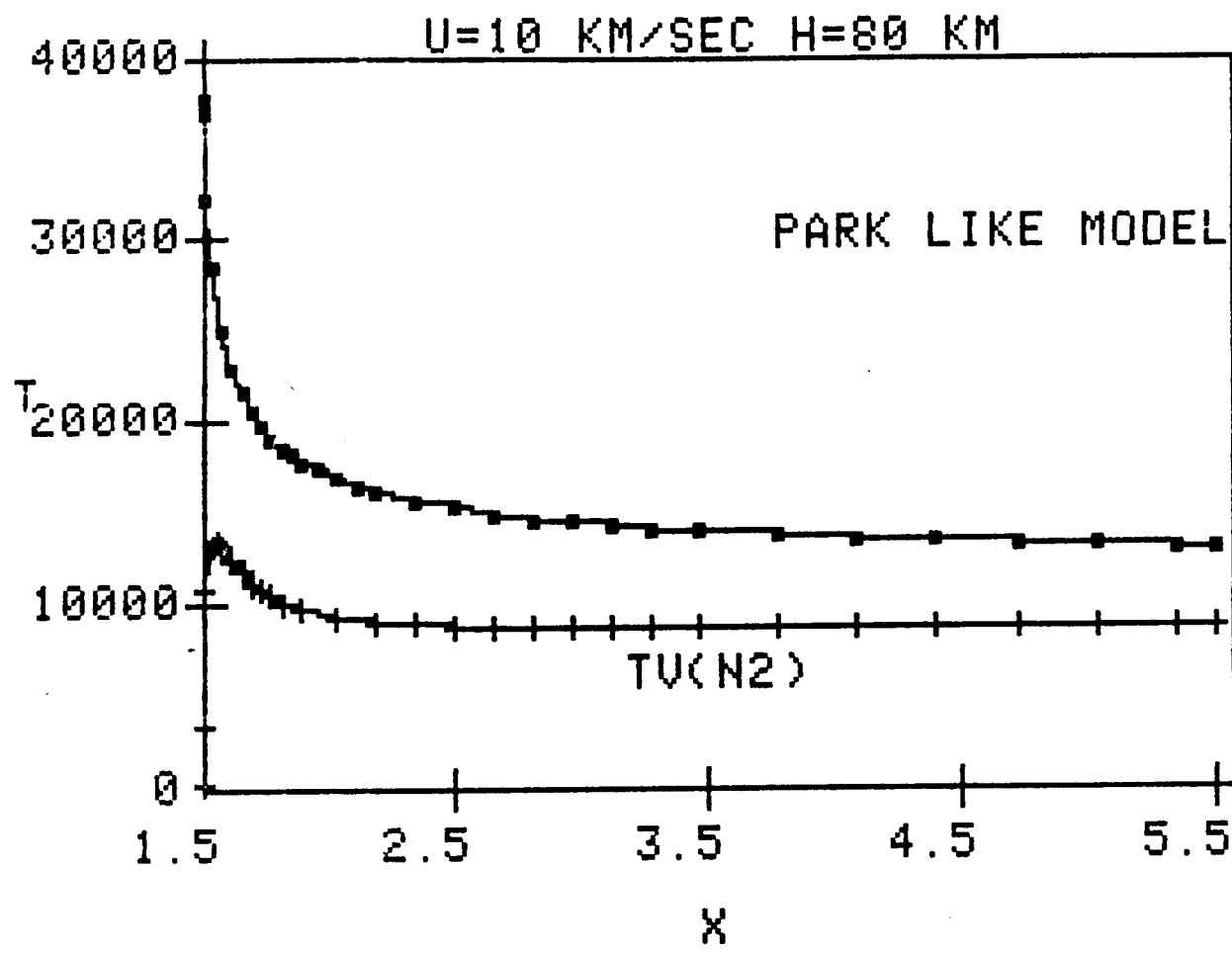


Figure 6 -- Temperature Profiles Along Streamline XS=1.5  
(Park Like Model)

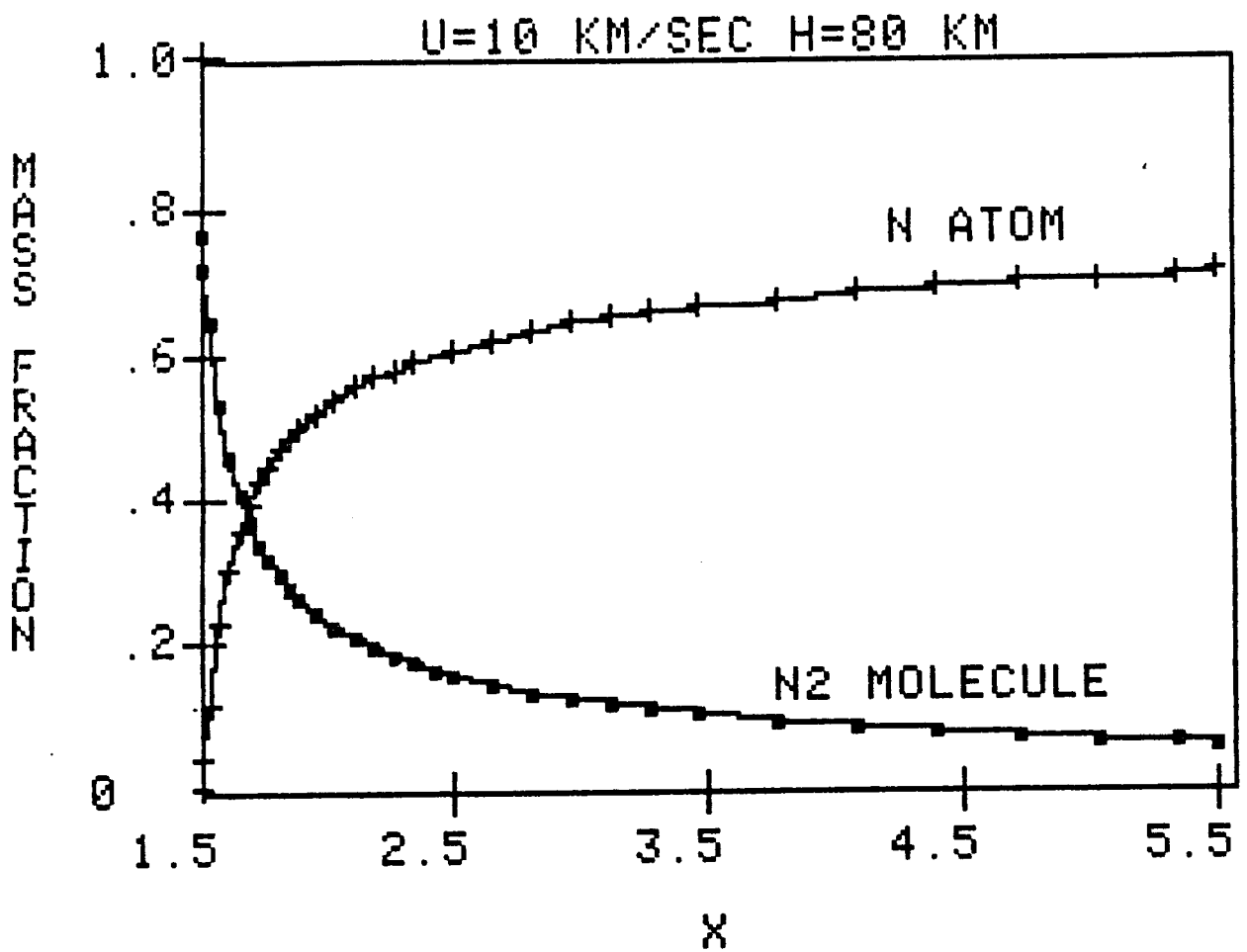


Figure 7 -- Concentration Profiles Along Streamline XS=1.5  
(Park Like Coupling Model)

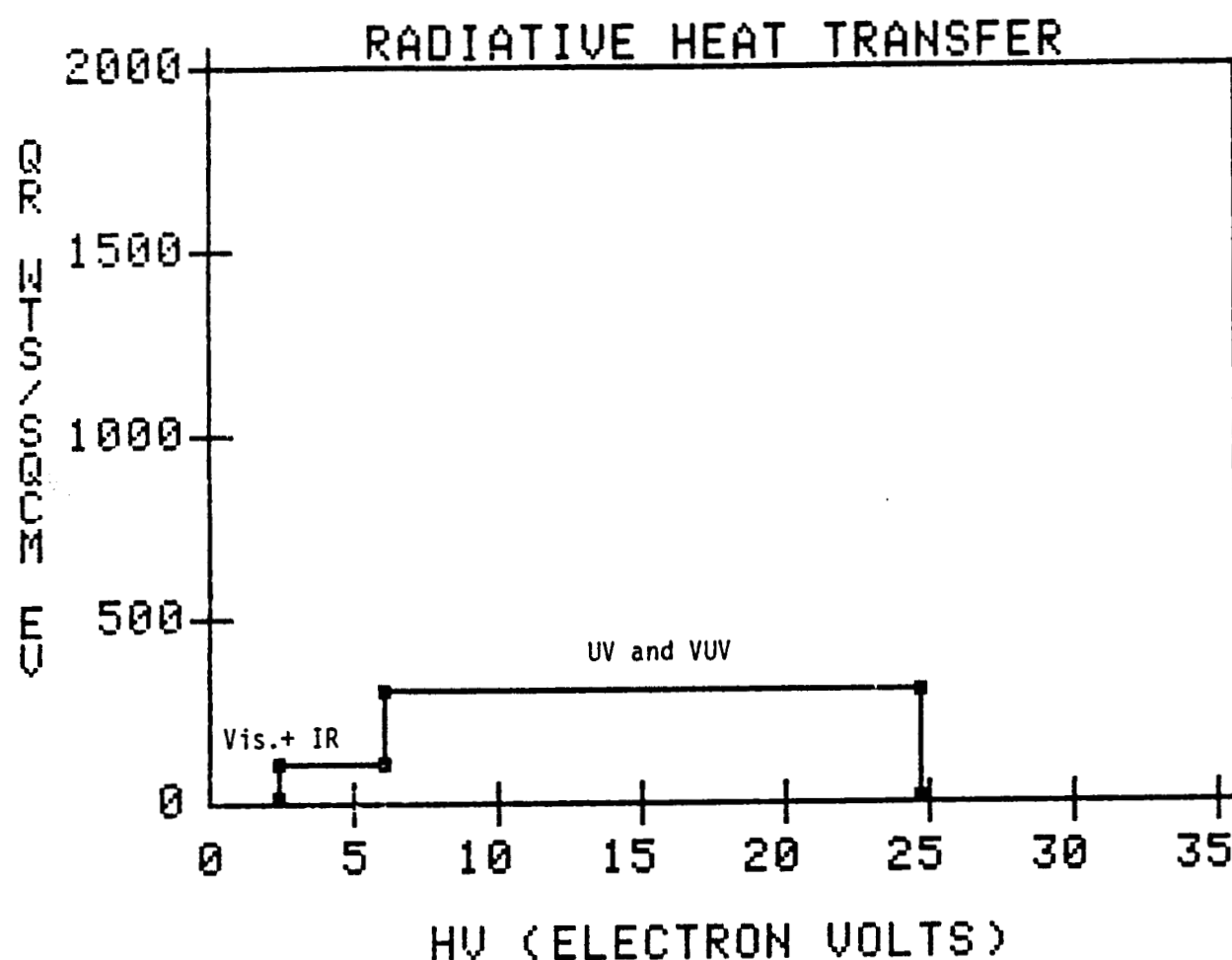


Figure 8 -- Spectral Variation of Wall Radiative Heat Transfer at 9 cm Above Centerline (Radiance Non-Absorbing Model)

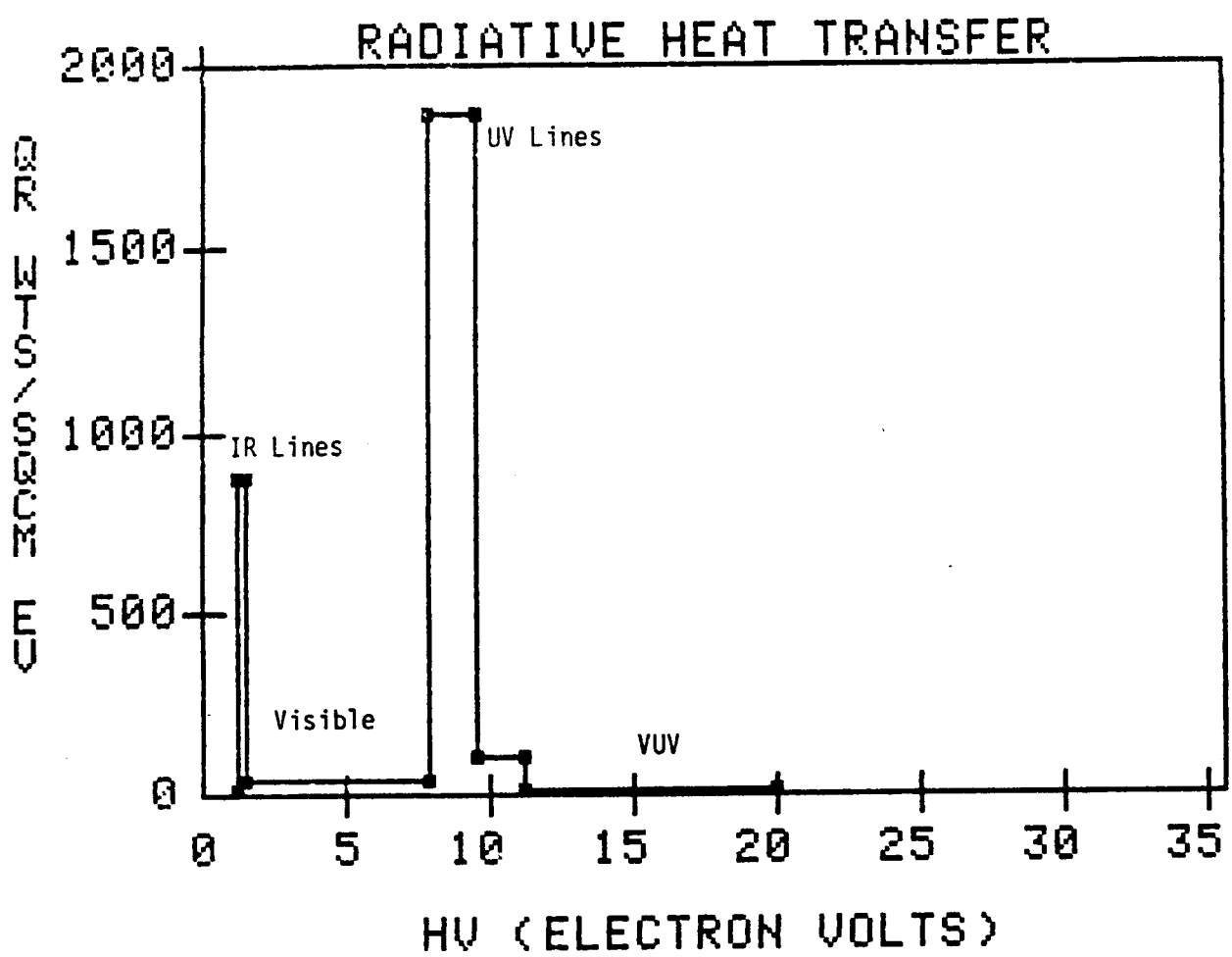


Figure 9 -- Spectral Variation of Wall Radiative Heat Transfer at 9 cm Above Centerline (5 Step Absorption Coefficient Model)

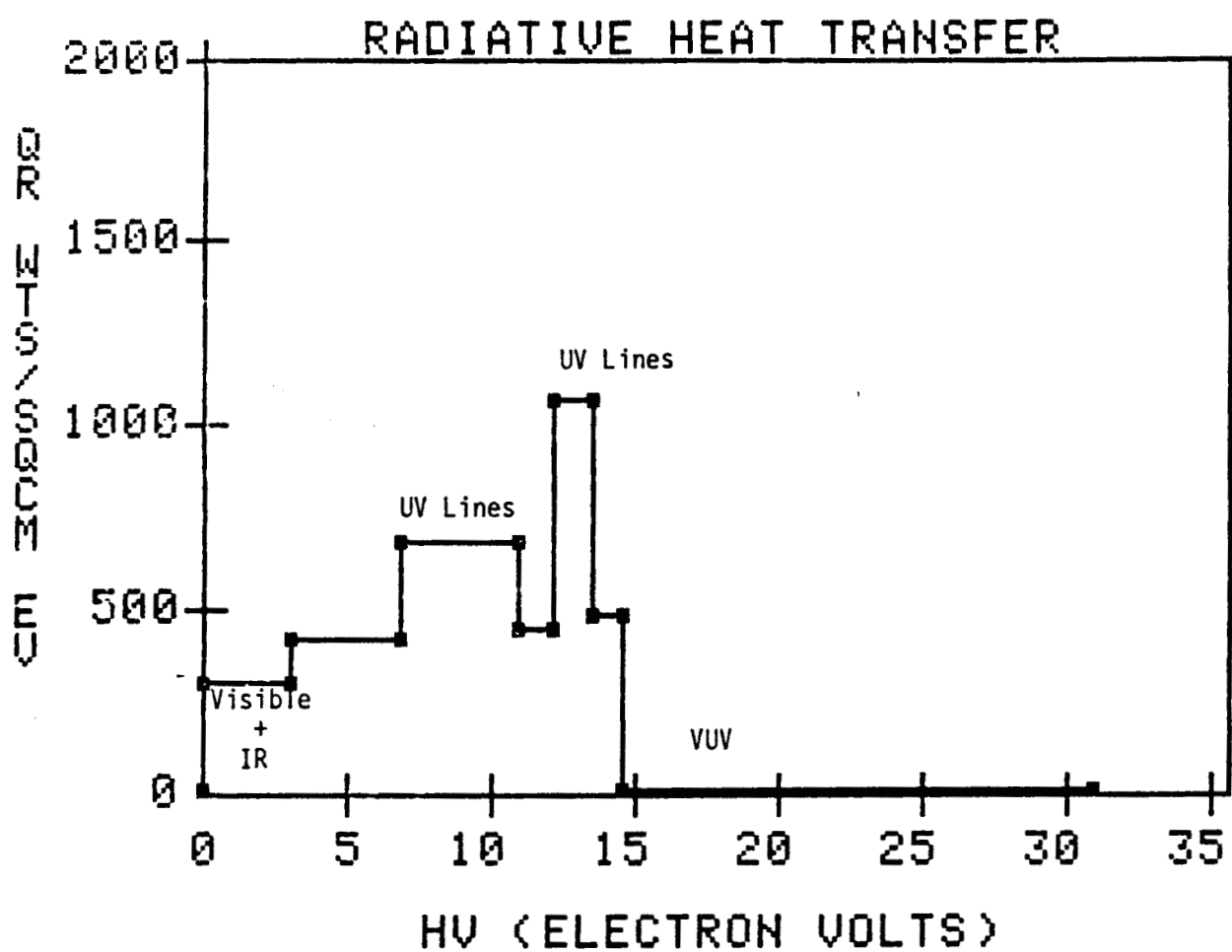


Figure 10 -- Spectral Variation of Wall Radiative Heat Transfer at 9 cm Above Centerline (8 Step Absorption Coefficient Model)